The self-similar topology of passive interfaces advected by two-dimensional turbulent-like flows

J. C. Vassilicos and J. C. H. Fung

Citation: Physics of Fluids **7**, 1970 (1995); doi: 10.1063/1.868510
View online: http://dx.doi.org/10.1063/1.868510
View Table of Contents: http://scitation.aip.org/content/aip/journal/pof2/7/8?ver=pdfcov
Published by the AIP Publishing

Articles you may be interested in

Scaling and self-similarity in two-dimensional hydrodynamics
Chaos **25**, 075404 (2015); 10.1063/1.4913852

Self-similarity in decaying two-dimensional stably stratified adjustment
Phys. Fluids **19**, 036603 (2007); 10.1063/1.2717514

Self-similar clustering of inertial particles and zero-acceleration points in fully developed two-dimensional turbulence
Phys. Fluids **18**, 115103 (2006); 10.1063/1.2364263

Dynamics of passively advected impurities in simple two-dimensional flow models
Phys. Fluids A **4**, 1805 (1992); 10.1063/1.858402

The generation of vortices in high-resolution, two-dimensional decaying turbulence and the influence of initial conditions on the breaking of self-similarity
Phys. Fluids A **1**, 1027 (1989); 10.1063/1.857393

Did your publisher get
18 MILLION DOWNLOADS in 2014?
AIP Publishing did.

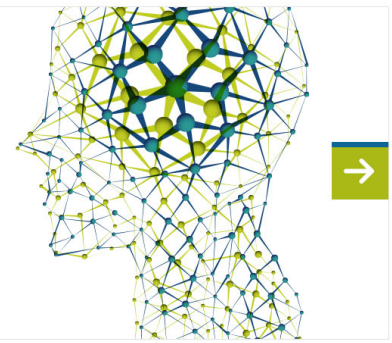

AIP Publishing THERE'S POWER IN NUMBERS. Reach the world with AIP Publishing.

This article is copyrighted as indicated in the article. Reuse of AIP content is subject to the terms at: http://scitation.aip.org/termsconditions. Downloaded to IP: 155.198.172.98 On: Fri, 12 Jun 2015 13:29:57

The self-similar topology of passive interfaces advected by two-dimensional turbulent-like flows

J. C. Vassilicos
Department of Applied Mathematics and Theoretical Physics, University of Cambridge, Silver Street, Cambridge CB3 9EW, United Kingdom

J. C. H. Fung
Department of Mathematics, The Hong Kong University of Science and Technology, Clear Water Bay, Hong Kong

(Received 3 August 1994; accepted 12 April 1995)

We study the topology, and in particular the self-similar and space-filling properties of the topology of line-interfaces passively advected by five different 2-D turbulent-like velocity fields. Special attention is given to three fundamental aspects of the flow: the time unsteadiness, the classification of local spatial flow structure in terms of hyperbolic and elliptic points borrowed from the study of phase spaces in dynamical systems and a classification of flow structure in wavenumber space derived from the studies of Weierstrass and related functions. The methods of analysis are based on a classification of interfacial scaling topologies in terms of K- and H- fractals, and on two interfacial scaling exponents, the Kolmogorov capacity D_K and the dimension D introduced by Fung and Vassilicos [Phys. Fluids **11**, 2725 (1991)] who conjectured that $D>1$ implies that the interface is H-fractal. An argument is presented (in the Appendix) to show that $D>1$ is a necessary condition for the evolving interface to be H-fractal through the action of the flow, and that $D>1$ is also sufficient provided that no isolated regions exist where the flow velocity is either unbounded or undefined in finite time. D is interpreted to be a degree of H-fractality and is different from the Hausdorff dimension D_H. In all our flows, steady and unsteady, interfaces in particular realisations of the flow reach a non-space-filling steady self-similar state where D and D_K are both constant in time even though the interface continues to be advected and deformed by the flow. It is found that D is equal to 1 in 2-D steady flows and always increases with unsteadiness, that D_K generally decreases with unsteadiness where the interfacial topology is dominated by spirals, and that D_K increases with unsteadiness where the interfacial topology is dominated by tendrils. In those flows with larger number of modes, D_K is a non-increasing function of unsteadiness and a decreasing function of the exponent p of the flow's self-similar energy spectrum $E(k)\sim k^{-p}$. D_K's decreasing dependences on unsteadiness and the exponent p can be explained by the presence of spirals in the eddy regions of the flow. The values of D and D_K and their dependence on unsteadiness can change significantly only by changing the distribution of wavenumbers in wavenumber space while keeping the phases and energy spectrum constant. © *1995 American Institute of Physics.*

I. INTRODUCTION

Laboratory experiments with different types of interfaces in a large variety of turbulent flows e.g.: turbulent/non-turbulent interfaces, scalar and vorticity interfaces in boundary layers, in axisymmetric jets, in plane wakes or in mixing layers, dissipative structures in fully developed turbulence, premixed turbulent flamelets, etc. (Sreenivasan *et al.*,[1] Sreenivasan,[2] North and Santavicca,[3] Sakai *et al.*,[4] Villermaux[5]) have shown that the Kolmogorov capacity D_K (often misleadingly called fractal dimension) of these interfaces can often be defined and is a non-integer. This is evidence that interfaces in turbulence are somehow self-similar, but the meaning of that self-similarity remains unclear, in particular the geometrical and topological structures implied on these interfaces.

Vassilicos and Hunt[6] introduced a distinction between two different scaling topologies: K-fractals and H-fractals. A generic example of a K-fractal is the spiral curve $r(\phi)\sim\phi^{-a}$ (in cylindrical coordinates where r is the distance to the centre of the spiral and ϕ is an angle); the Kolmogorov capacity D_K of that spiral is a direct function of the exponent a and is larger than 1. However, the Hausdorff dimension D_H of any single spiral is always $D_H=1$ because the geometry of a spiral is *smooth* everywhere except at its centre. It is the accumulation of length scales at the spiral's centre that causes D_K to be larger than 1, but such an isolated singularity is not enough for D_H to be larger than 1; instead, an uncountable set of non-isolated singularities is needed so that $D_H>1$, in which case the geometry is H-fractal and is nearly everywhere irregular. A curve is K-fractal and its self-similarity is local when $D_K>1$ and $D_H=1$, but is H-fractal and its self-similarity is global when $D_K>1$ and $D_H>1$. When $D_K=D_H=1$, the curve is smooth absolutely everywhere. Thus, the scaling exponents D_K and D_H lead to a classification of interfaces with different scaling topologies. Other related exponents can also be used in such a classification, such as D'_K and D'_H, the Kolmogorov capacity and the Hausdorff dimension of the point-intersections of the interface with a straight line (Vassilicos and Hunt[6]).

The distinction between K- and H-fractals is not just an academic clarification. It can have important consequences,

 1070-6631/95/7(8)/1970/29/$6.00 © 1995 American Institute of Physics

This article is copyrighted as indicated in the article. Reuse of AIP content is subject to the terms at: http://scitation.aip.org/termsconditions. Downloaded to IP: 155.198.172.98 On: Fri, 12 Jun 2015 13:29:57

for example, in pollutant dispersion, in the mixing of chemically reacting fluids, and in combustion. Two interfaces, one H-fractal and one K-fractal that have the same value of D_K, can nevertheless have very different surface areas. More dramatically, two different interfaces with the same value of D'_K may have respectively a finite and an infinite surface area per unit volume if the one is K-fractal and the other H-fractal!

The turbulent flame speed of a flame interface will therefore be much different according to whether the flame is K-fractal or H-fractal. In fact, if the interface becomes K-fractal as a result of the turbulence, then it may be expected that the turbulence enhances the burning to a lesser degree than a reasoning based on the Richardson cascade (and which implicitly assumes the interface to be H-fractal) would suggest.

This reasoning is founded on the self-similarity of the Richardson cascade of eddies, and is essentially a statistical argument that ignores the structure of the turbulence. Each eddy of the cascade is assumed to create a wrinkle or contortion on the interface of the same wavelength as the eddy itself; the collective action of all these self-similar eddies of different sizes induces a self-similar cascade of deformations on the interface which may remind one of the geometry of a H-fractal. No structural nor geometrical information is used in this argument (e.g. how are the eddies distributed in space, what is the nature of the *shape* of the wrinkles produced by these eddies on the interface, how are these wrinkles structured on the interface); it is a purely statistical argument. The most important conclusion that can be drawn from this argument, is that an interface cannot have a characteristic length scale of deformations within the range of length scales where the turbulence has no characteristic scale of motion (the range of length scales of the Richardson cascade). However, the self-similarity implied can be either local or global, and the geometry of the interface must reflect, to some extent, the structure and topology of the turbulence.

Wray and Hunt[7] have classified turbulent structure, essentially, as follows (see Fig. 1): (1) *eddy* regions, which are strong swirling regions with vorticity; (2) *convergence* regions surrounding a saddle point where there is irrotational straining (in these regions there is convergence of streamlines), and (3) *streaming* regions where the flow is very weakly curved and runs rather fast.

In a totally different context, Berry *et al.*[8] have made a first attempt to classify the convolutions of curves in phase planes evolving under the action of continuous area-preserving maps. They point out that the complexity of these curves is totally due to the fixed points of the map. These are the elliptic and the hyperbolic points whose analogues in flows are respectively the eddy and the convergence regions. Berry *et al.*[8] argue that the only possible contortions of the curve are either 'whorls' (spiral structures) when the curve is in the vicinity of an elliptic point, or 'tendrils' when the curve is in the vicinity of an hyperbolic point. In the same spirit, a line in any incompressible fluid flow can also only develop either 'whorls' or 'tendrils', and thereby have either a K- or a H-fractal topology, possibly in different regions of the flow. Unfortunately the relation between a classification of spatial flow or streamline structure and a classification of interfacial scaling topology is not straightforward because, as expected from previous studies of chaotic advection (see Ottino[9] and Fung and Vassilicos[10]), the unsteadiness of the flow has an important influence on the topology and scaling of the interface.

In this paper we investigate the relation between the self-similar topology of lines passively advected by a 2-D turbulent-like velocity field $\mathbf{u}(\mathbf{x},t)$ and the structure of $\mathbf{u}(\mathbf{x},t)$ in the physical and wavenumber spaces and in time. Following Kraichnan,[11] Drummond *et al.*,[12] Turfus,[13] Maxey and Corrsin,[14] Maxey[15] and Fung *et al.*[16] we simulate $\mathbf{u}(\mathbf{x},t)$ by summing different Fourier modes with a prescribed self-similar energy spectrum. The eddy, convergence and streaming regions are clearly reproduced by the streamline pattern of such velocity fields (see Fig. 1), and the variation of $|\mathbf{u}(\mathbf{x},t)|$ along and across streamlines depends on the energy spectrum. Furthermore, the study of 1-D Weierstrass functions (Falconer[17]) demonstrates that two velocity profiles with identical energy spectra can be qualitatively different if the energy is distributed along different excited wavenumbers. Can this distribution of energy affect the topology of passively advected interfaces, even when the form of the energy spectrum is kept constant? But first of all, does the topology of the interface reach a self-similar stationary state even when the interface continues to stretch and fold, and if so, how does the interfacial scaling vary with the energy spectrum, with the topology of streamlines and with the unsteadiness of the velocity field?

It is often assumed that the interfacial surface area is a simple function of a 'fractal' dimension of the surface, which in turn, is either a universal constant or an exponent that can be easily deduced from a simple statistical argument involving the Richardson cascade of eddy motions and various fluxes across the interface when the flow is fully developed equilibrium isotropic turbulence (Sreenivasan *et al.*,[2] Peters[18]). The present study shows how the general relation between the interfacial scaling, topology and surface area on the one hand, and the structure of the velocity field on the other, involves various subtle aspects of the flow and its topology that cannot be accounted for by traditional statistical scaling arguments. However, it is shown that the topology of the interface does reach an asymptotic equilibrium self-similar state in the turbulent-like flows considered here even though classical equilibrium arguments do not apply to these flows, and the relation between a couple of steady scaling exponents of the evolving interface with various properties and parameters of the velocity field is investigated. When are the scaling properties of the interface dominated by the space structure, the time structure or the wavenumber structure of a flow?

In the next section we describe how we simulate 2-D turbulent-like velocity fields $\mathbf{u}(\mathbf{x},t)$, and how we measure two different interfacial scaling exponents, the Kolmogorov capacity D_K and the dimension D introduced by Fung and Vassilicos.[10] A table summarising the main properties of all the velocity fields used here can be found in section II.E. In

This article is copyrighted as indicated in the article. Reuse of AIP content is subject to the terms at: http://scitation.aip.org/termsconditions. Downloaded to IP: 155.198.172.98 On: Fri, 12 Jun 2015 13:29:57

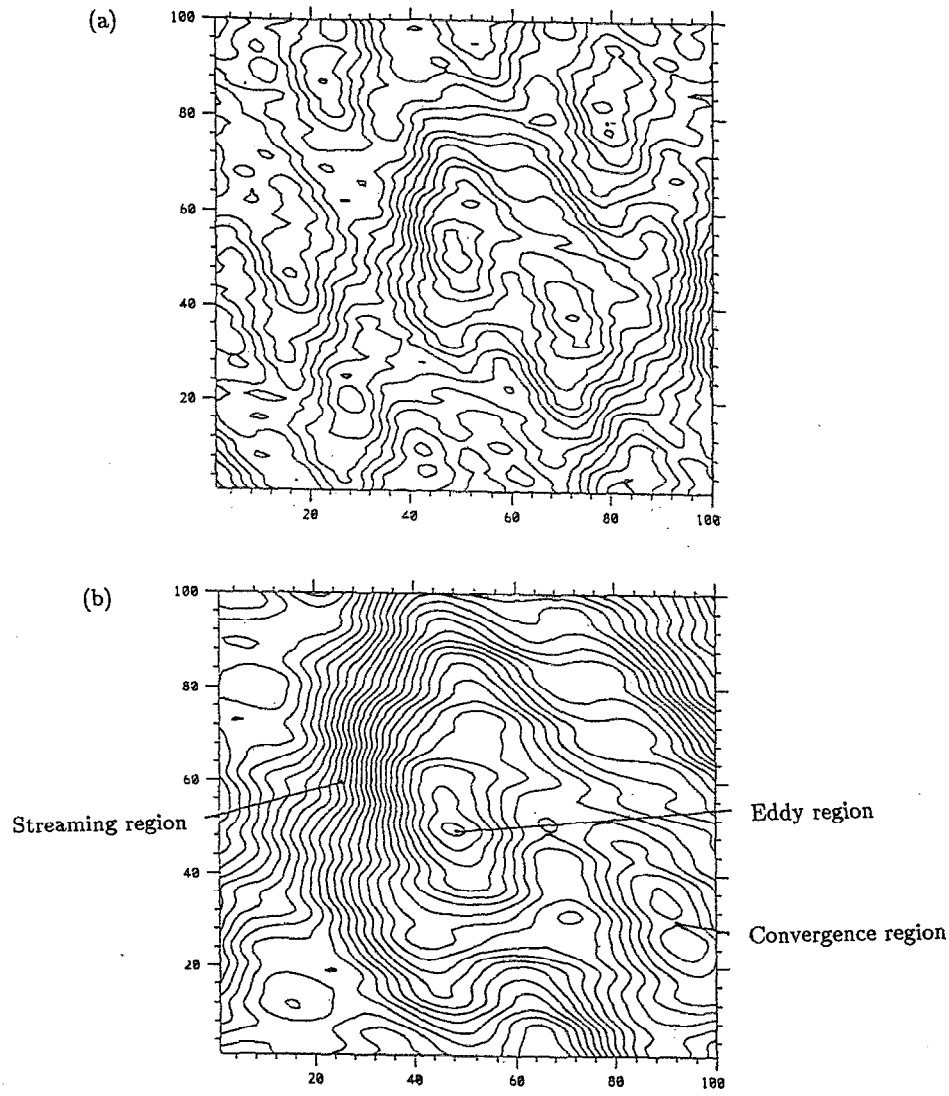

FIG. 1. Streamline plots showing the three different types of regions that constitute the flow. The number 100 corresponds to two integral length scales L_T of the velocity field. (a) $E(k)\sim k^{-3.2}$, (b) $E(k)\sim k^{-3.6}$.

section III we present our results on the scaling topology of lines advected by 2-D turbulent-like flows, and we conclude in section IV.

II. THE VELOCITY FIELDS AND THE SCALING EXPONENTS

A. General properties

We need a velocity field where the energy spectrum and the distribution of excited modes can be changed at will, thus enabling a study of the relation between the structure of the velocity field and the structure of passive interfaces advected by the turbulence. The velocity fields we use, are not approximations of a small-scale turbulent solution of the Navier–Stokes equations, but are easily implemented on a computer, and have several common features with such solutions; they have a self-similar energy spectrum over a large range of scales, and their flow structure can be classified in terms of eddy, convergence and streaming regions (Wray and Hunt,[7] Fung *et al.*[19]).

Homogeneous incompressible turbulence $\mathbf{u}(\mathbf{x},t)$ is traditionally studied in the Fourier representation

$$\mathbf{u}(\mathbf{x},t)=\int \{\mathbf{A}(\mathbf{k},t)\cos[\mathbf{k}\cdot\mathbf{x}+\psi(\mathbf{k})]+\mathbf{B}(\mathbf{k},t)\sin[\mathbf{k}\cdot\mathbf{x}+\psi(\mathbf{k})]\}\,d\mathbf{k}, \tag{1}$$

where

$$\mathbf{A}(\mathbf{k},t)=\mathbf{A}(-\mathbf{k},t), \tag{2a}$$

$$\mathbf{B}(\mathbf{k},t)=-\mathbf{B}(-\mathbf{k},t), \tag{2b}$$

$$\psi(\mathbf{k})=-\psi(-\mathbf{k}) \tag{2c}$$

and incompressibility implies

This article is copyrighted as indicated in the article. Reuse of AIP content is subject to the terms at: http://scitation.aip.org/termsconditions. Downloaded to IP: 155.198.172.98 On: Fri, 12 Jun 2015 13:29:57

$$\mathbf{A}(\mathbf{k},t)\cdot\mathbf{k}=\mathbf{B}(\mathbf{k},t)\cdot\mathbf{k}=0. \tag{3}$$

Following original ideas by Kraichnan,[11] Drummond *et al.*,[12] Turfus[13] and Fung *et al.*[16] simulate turbulent-like velocity fields by adding random Fourier modes together rather than solving the Navier–Stokes equations for large Reynolds numbers Re. This approach, now referred to as 'Kinematic Simulation', essentially consists of numerically integrating (1) and picking the vectors $\mathbf{A}(\mathbf{k},t)$ and $\mathbf{B}(\mathbf{k},t)$ randomly from a probability distribution that is consistent with some characteristic properties of incompressible turbulence. The main property of high Re turbulence that we want to keep is the self-similar form of the power spectrum which specifies the amplitudes of the vectors $\mathbf{A}(\mathbf{k},t)$ and $\mathbf{B}(\mathbf{k},t)$; their directions are chosen randomly from a uniform distribution.

We require zero-mean flow velocity, that is $\int \mathbf{u}\, d\mathbf{x}=0$, for which it is sufficient and necessary that $\mathbf{A}(\mathbf{k}=0,\,t)=\mathbf{B}(\mathbf{k}=0,\,t)=0$. We set the amplitudes of $\mathbf{A}(\mathbf{k},t)$ and $\mathbf{B}(\mathbf{k},t)$ to be equal to each other and independent of time. Therefore,

$$|\mathbf{A}(\mathbf{k},t)|=|\mathbf{B}(\mathbf{k},t)|, \tag{4}$$

which we set equal to the modulus of a function $U(k)$, i.e. $|\mathbf{A}(\mathbf{k},t)|=|\mathbf{B}(\mathbf{k},t)|=|U(k)|$; the amplitudes of $\mathbf{A}(\mathbf{k},t)$ and $\mathbf{B}(\mathbf{k},t)$ are determined by choosing $U(k)$ in accordance with a specified energy spectrum.

The Fourier transform of $\mathbf{A}(\mathbf{k},t)+i\mathbf{B}(\mathbf{k},t)$ with respect to time is

$$\tilde{\mathbf{A}}(\mathbf{k},\omega)+i\tilde{\mathbf{B}}(\mathbf{k},\omega)=\frac{1}{2\pi}\int e^{-i\omega t}[\mathbf{A}(\mathbf{k},t)+i\mathbf{B}(\mathbf{k},t)]\, dt \tag{5}$$

and is such that

$$\mathbf{k}\cdot\tilde{\mathbf{A}}(\mathbf{k},\omega)=\mathbf{k}\cdot\tilde{\mathbf{B}}(\mathbf{k},\omega)=0 \tag{6}$$

because of (2).

As $\mathbf{A}(\mathbf{k},t)+i\mathbf{B}(\mathbf{k},t)$ and $\tilde{\mathbf{A}}(\mathbf{k},\omega)+i\tilde{\mathbf{B}}(\mathbf{k},\omega)$ are 2-D vectors, a particular consequence of (3) and (6) is that $\tilde{\mathbf{A}}(\mathbf{k},\omega)+i\tilde{\mathbf{B}}(\mathbf{k},\omega)$ and $\mathbf{A}(\mathbf{k},t)+i\mathbf{B}(\mathbf{k},t)$ are parallel, so that $\tilde{\mathbf{A}}(\mathbf{k},\omega)+i\tilde{\mathbf{B}}(\mathbf{k},\omega)$ can be written in the following general form:

$$\tilde{\mathbf{A}}(\mathbf{k},\omega)+i\tilde{\mathbf{B}}(\mathbf{k},\omega)=[\mathbf{A}(\mathbf{k})+i\mathbf{B}(\mathbf{k})]P(\omega,\mathbf{k}), \tag{7a}$$

where $\mathbf{A}(\mathbf{k})+i\mathbf{B}(\mathbf{k})=\mathbf{A}(\mathbf{k},t=0)+i\mathbf{B}(\mathbf{k},t=0)$ and $P(\omega,\mathbf{k})$ is a function of ω and $\mathbf{k}$ such that

$$P^*(\omega,\mathbf{k})=P(-\omega,-\mathbf{k}) \tag{7b}$$

in order to satisfy (2a) and (2b).

Taking the Fourier transform of both sides of (7a) with respect to ω one obtains

$$\mathbf{A}(\mathbf{k},t)+i\mathbf{B}(\mathbf{k},t)=[\mathbf{A}(\mathbf{k})+i\mathbf{B}(\mathbf{k})]\int P(\omega,\mathbf{k})e^{i\omega t}\, d\omega. \tag{8}$$

Then taking the norm of both sides of (8) and making use of the constancy of $U(k)$ over time we get

$$\int P(\omega,\mathbf{k})P^*(\omega+\Omega,\mathbf{k})\, d\omega=\delta(\Omega). \tag{9}$$

Also, by setting $t=0$ in (8) it follows that

$$\int P(\omega,\mathbf{k})\, d\omega=1. \tag{10}$$

A simple and straightforward solution to (9) and (10) under the constraint (7b) is

$$P(\omega,\mathbf{k})=\delta(\omega-\omega(\mathbf{k})), \tag{11}$$

where $\omega(\mathbf{k})=s(\mathbf{k})\omega_k$; $s(\mathbf{k})=\pm 1$ and is such that $s(\mathbf{k})=-s(-\mathbf{k})$, and ω_k is *a priori* an arbitrary function of k, and is the frequency of the unsteadiness of the Fourier modes of wavenumber k.

It now follows that

$$\mathbf{A}(\mathbf{k},t)+i\mathbf{B}(\mathbf{k},t)=[\mathbf{A}(\mathbf{k})+i\mathbf{B}(\mathbf{k})]e^{i\omega(\mathbf{k})t} \tag{12}$$

and standard algebra leads from (1) to

$$\mathbf{u}(\mathbf{x},t)=\int\{\mathbf{A}(\mathbf{k})\cos[\mathbf{k}\cdot\mathbf{x}+\omega(\mathbf{k})t+\psi(\mathbf{k})]+\mathbf{B}(\mathbf{k})\sin[\mathbf{k}\cdot\mathbf{x}+\omega(\mathbf{k})t+\psi(\mathbf{k})]\}\, d\mathbf{k}. \tag{13}$$

A numerical implementation of $\mathbf{u}(\mathbf{x},t)$ requires a discretisation of (13), that is,

$$\mathbf{u}(\mathbf{x},t)=\sum_{n=1}^{N_k}\sum_{m=1}^{M_\phi}\Delta k_n\Delta\phi_m k_n[\mathbf{A}_{nm}\cos(\mathbf{k}_{nm}\cdot\mathbf{x}+\omega_{nm}t+\psi_{nm})+\mathbf{B}_{nm}\sin(\mathbf{k}_{nm}\cdot\mathbf{x}+\omega_{nm}t+\psi_{nm})], \tag{14}$$

where $\mathbf{k}_{nm}=k_n(\cos\phi_m,\sin\phi_m)$, $\mathbf{A}_{nm}=\mathbf{A}(\mathbf{k}_{nm})$, $\mathbf{B}_{nm}=\mathbf{B}(\mathbf{k}_{nm})$, $\omega_{nm}=\omega(\mathbf{k}_{nm})$ and $\psi_{nm}=\psi(\mathbf{k}_{nm})$. The choice of discretization is a choice of N_k, M_ϕ, Δk_n, $\Delta\phi_m$, k_n and ϕ_m. We set $\psi_{nm}=0$, and we always take one mode per wavenumber k_n, i.e. $M_\phi=1$ and $\Delta\phi_m=2\pi$; thus, there is only one phase ϕ_m per wavenumber and ϕ_m may be replaced by $\phi_n=\phi(k_n)$. Hence, (14) reduces to

$$\mathbf{u}(\mathbf{x},t)=2\pi\sum_{n=1}^{N_k}\Delta k_n k_n[\mathbf{A}_n\cos(\mathbf{k}_n\cdot\mathbf{x}+\omega_n t)+\mathbf{B}_n\sin(\mathbf{k}_n\cdot\mathbf{x}+\omega_n t)]. \tag{15}$$

Because of (6) and because the flow is two-dimensional, $\mathbf{A}_n=\pm\mathbf{B}_n$ in the direction perpendicular to $\mathbf{k}_n$. Since $\mathbf{k}_n=k_n(\cos\phi_n,\sin\phi_n)$, it follows that $\mathbf{A}_n=\pm A_n(\sin\phi_n,-\cos\phi_n)$ and $\mathbf{B}_n=\pm A_n(\sin\phi_n,-\cos\phi_n)$. The $\pm$ signs are arbitrary, as are the angles ϕ_n. We pick these signs and $s(k_n)$ randomly among $+1$ and -1, and the random phases ϕ_n are drawn from a uniform distribution between 0 and 2π.

B. Stationarity and unsteadiness of the velocity fields and the energy spectrum

The velocity field in the form (13) is stationary in the sense that

$$\frac{\partial}{\partial t}\int \mathbf{u}(\mathbf{x},t)\cdot\mathbf{u}(\mathbf{x},t+\tau)\, d\mathbf{x}=0 \tag{16}$$

for all values of τ, in particular $\tau=0$. The total kinetic energy of a velocity field $\mathbf{u}(\mathbf{x},t)$ corresponds to the case $\tau=0$

This article is copyrighted as indicated in the article. Reuse of AIP content is subject to the terms at: http://scitation.aip.org/termsconditions. Downloaded to IP: 155.198.172.98 On: Fri, 12 Jun 2015 13:29:57

and is $E_\rho = \frac{1}{2}\int \rho \mathbf{u}(\mathbf{x},t)\cdot\mathbf{u}(\mathbf{x},t)\, d\mathbf{x}$ (where ρ is the density of the fluid which we assume to be constant in space); therefore

$$E_\rho = 4\rho\pi^3 \int [|\mathbf{A}(\mathbf{k},t)|^2 + |\mathbf{B}(\mathbf{k},t)|^2] k\, dk$$

$$= 8\pi^3 \rho \int kU^2(k)\, dk. \tag{17}$$

The total kinetic energy of the system is conserved because U does not depend on time. Thus, the energy spectrum is also independent of time and can be related to the amplitude $U(k)$ in two different ways. Either by taking a deterministic point of view (as in Vassilicos[20,21]), in which case the power spectrum $E(k)$ is

$$E(k) = \frac{1}{\rho} E_\rho(k) = 8\pi^3 k U^2(k), \tag{18}$$

or by taking a statistical point of view (as in Fung *et al.*[16]), in which case the *ensemble*-average kinetic energy per unit mass at each wavenumber must equal that in the specified power spectrum $E(k)$:

$$\langle U^2(k_n)\rangle k_n \Delta k_n = 2\int_{k_n}^{k_{n+1}} E(k)\, dk \approx 2E(k_n)\Delta k_n, \tag{19}$$

where $\langle\ \rangle$ denotes the ensemble average over many realizations of the flow field. [Note that $E_\rho(k)$ has the same dimensions as $\rho E(k)$.]

If we make the deterministic choice (18), then, for the velocity field to be self-similar in the sense that $E(k)\sim k^{-p}$, $\mathbf{A}(\mathbf{k},t)$ and $\mathbf{B}(\mathbf{k},t)$ have to be chosen so that $|U(k)|\sim k^{-(1+p)/2}$. If, on the other hand, we make the stochastic choice (19), then we draw $U(k_n)$ from a probability distribution where the mean is zero and the variance $\langle U^2(k_n)\rangle$ is given by (19). The self-similarity of the velocity field is introduced by setting $E(k)\sim k^{-p}$ in (19).

Even though the flow fields are stationary in the sense that their energy spectra remain constant in time, the flows can evolve so that streamlines may be different at different times. This is the *unsteadiness* of the flow field (15) which is tuned in by choosing finite unsteadiness frequencies $\omega_n = \omega(\mathbf{k}_n) = s(\mathbf{k}_n)\omega_{k_n}$. Once again, two different choices will be made in the present work: either we assume that a wavemode travels at a speed proportional to $U(k)$, in which case

$$\omega_k = \lambda k U(k) \sim k^{(1-p)/2} \tag{20}$$

and the constant λ is not dimensionless, or we assume that the unsteadiness frequency is proportional to the eddy turnover frequency, i.e.

$$\omega_k = \lambda [k^3 E(k)]^{\frac{1}{2}} \sim k^{(3-p)/2}, \tag{21}$$

where λ is dimensionless. [If $\lambda \ll 1$, then the velocity field $\mathbf{u}(\mathbf{x},t)$ is approximately steady. If, on the other hand, $\lambda \gg 1$, then the velocity field is essentially random. Turbulence is neither random nor steady, and therefore we expect λ to be order 1 in a turbulent-like flow.]

In the sequel, when we use an unsteadiness of the type (20), the values of p range between 3 and 4, in which case ω_k is a decreasing function of k (an equilibrium theory by Kraichnan[22] and Batchelor[23] gives $p=3$ for 2-D turbulence, whilst Saffman[24] obtains $p=4$ for 2-D well-separated patches of vorticity at large Reynolds number). On the other hand, when we use an unsteadiness of the type (21), p ranges between 1 and 3, so that ω_k is a non-decreasing function of k. That way we experiment with two qualitatively different types of unsteadiness, and study whether they have different effects on the topology of the evolving interface.

C. Discretisation and the Weierstrass function

It is beneficial to review a few properties of the Weierstrass function before proceeding with the details of the velocity field's discretisation. A 1-D Weierstrass function $u(x)$ is defined as follows:

$$u(x) = \sum_{n=1}^{+\infty} a_n \sin\left(\frac{2\pi x}{\lambda_n}\right), \tag{22}$$

where $a_n = a^n$, $0<a<1$ and $2\pi/\lambda_n = b^n$. When $ab>1$, $u(x)$ is nowhere differentiable and the graph $(x,u(x))$ is H-fractal with D_K and D_H larger than 1 (see Falconer[25] and Hardy[26]). This is not the case though when $ab<1$. For an intuitive understanding of this property, note that as $n\to\infty$, $a_n/\lambda_n \to \infty$ when $ab>1$, but $a_n/\lambda_n \to 0$ when $ab<1$.

One could also distribute a_n and λ_n algebraically, that is $a_n = n^{-\alpha}$, $k_n = 2\pi/\lambda_n = n^\beta$ where $\alpha,\beta>0$. To our knowledge such functions have not been thoroughly studied yet, with the only exception of the Riemann function (see Holschneider and Tchamitchian[27]) which corresponds to $\alpha=\beta=2$. Since $(a_n/\lambda_n)\sim n^{\beta-\alpha}$, we may expect very different qualitative behaviours when β is either smaller or larger than α; possibly an H-fractal behaviour when $\beta>\alpha$.

For the same self-similar power spectrum $a_n^2 \sim k_n^{-p}$, where $k_n = 2\pi/\lambda_n$, the Weierstrass function's geometrical distribution of wavemodes implies $a^2 b^p =$ Constant, and the algebraic distribution of wavemodes implies $p = 2\alpha/\beta$. For example, it is possible to have a $p=5/3$ power spectrum either with a geometric distribution or with an algebraic distribution. The type of function $u(x)$ may be qualitatively very different (K- or H-fractal) from one choice of wavemode distribution to the other even though the power spectrum remains unchanged.

It is therefore legitimate to ask whether, for a given energy spectrum, different discretisations or, equivalently, different distributions of modes can generate qualitatively different velocity fields, and whether these different velocity fields can generate qualitatively different interfacial topologies. The choice of discretisation is a choice of the n-dependence of k_n and Δk_n. Here we experiment with one algebraic and two geometric progressions of velocity wavemodes.

The choice of the two extreme values k_1 and k_{N_k} is essentially a choice of the range of length scales. With the only exception of the superimposed cellular flows (which we denote by SC, see section II.D), all the other velocity fields used here (denoted by DKS, SGKS and SAKS –these abbreviations are explained in the sequel) have two decades of wavenumbers; specifically, $k_1 = 1$ and $k_{N_k} = 100$.

This article is copyrighted as indicated in the article. Reuse of AIP content is subject to the terms at: http://scitation.aip.org/termsconditions. Downloaded to IP: 155.198.172.98 On: Fri, 12 Jun 2015 13:29:57

Furthermore, in DKS, SGKS and SAKS, $\Delta k_n=(k_{n+1}-k_{n-1})/2$ for $2\leqslant n\leqslant N_{k-1}$, and $\Delta k_1=(k_2-k_1)/2$, $\Delta k_{N_k}=(k_{N_k}-k_{N_k-1})/2$. It is easy to check that $\Sigma_{n=1}^{n=N_k}\Delta k_n=k_{N_k}-k_1$.

When we use the DKS ('Deterministic' Kinematic Simulation) velocity field where $|U(k)|$ is calculated deterministically from equation (18), the progression of wavenumbers is geometric. Because the fall-off of the self-similar energy spectrum is very sharp, most of the energy is concentrated near the smaller wavenumbers, and by distributing the k_n's geometrically most of the k_n's lie near k_1. Specifically, we choose $N_k=60$ and

$$k_n=(1+k_{n+1})/2 \tag{23}$$

for $2\leqslant n\leqslant 59$.

The velocity fields SAKS (Stochastic Algebraic Kinematic Simulation) and SGKS (Stochastic Geometric Kinematic Simulation) are labelled 'stochastic' in the sense that $U(k)$ is drawn from a probability distribution of zero mean and variance given by (19). For both these velocity fields, $N_k=100$. In SAKS, the distribution of wavenumbers k_n is an algebraic progression

$$k_n=k_1+cn(n-1)/2, \tag{24a}$$

where $c=2(k_{N_k}-k_1)/N_k(N_k-1)$. In SGKS, the distribution of wavenumbers is a geometric progression

$$k_n=a^{n-1}k_1, \tag{24b}$$

where $a=(k_{N_k}/k_1)^{1/(N_k-1)}$. Figure 2 shows how imperceptible the difference is between the energy distributions in SAKS and SGKS at the higher wavenumbers.

D. A superposition of cellular velocity fields (SC1 and SC2)

Stommel,[28] Maxey and Corrsin[14] and Maxey[15] have studied the gravitational settling of small, spherical particles in a convection cell flow. The flow is incompressible, steady and two-dimensional, and may be specified by a streamfunction $\psi(x,y)$ where

$$\psi(x,y)=\frac{U_0L}{\pi}\sin\left(\frac{\pi x}{L}\right)\sin\left(\frac{\pi y}{L}\right). \tag{25}$$

Streamlines are shown in Figs. 3(a-d). Such a flow arises in thermal convection with free-slip boundaries. The flow is composed of a periodic array of eddies in square cells of size L that extend in both the x and y directions. This flow field satisfies the inviscid Euler equations for steady flow; its velocity components in (x,y) coordinates aligned with the cell boundaries are

$$u=U_0\sin\left(\frac{\pi x}{L}\right)\cos\left(\frac{\pi y}{L}\right), \tag{26a}$$

$$v=-U_0\cos\left(\frac{\pi x}{L}\right)\sin\left(\frac{\pi y}{L}\right). \tag{26b}$$

A Lagrangian fluid element advected by this flow follows the simple path of a closed streamline in the steady flow and the value of ψ is a constant of the motion. However, Lagrangian

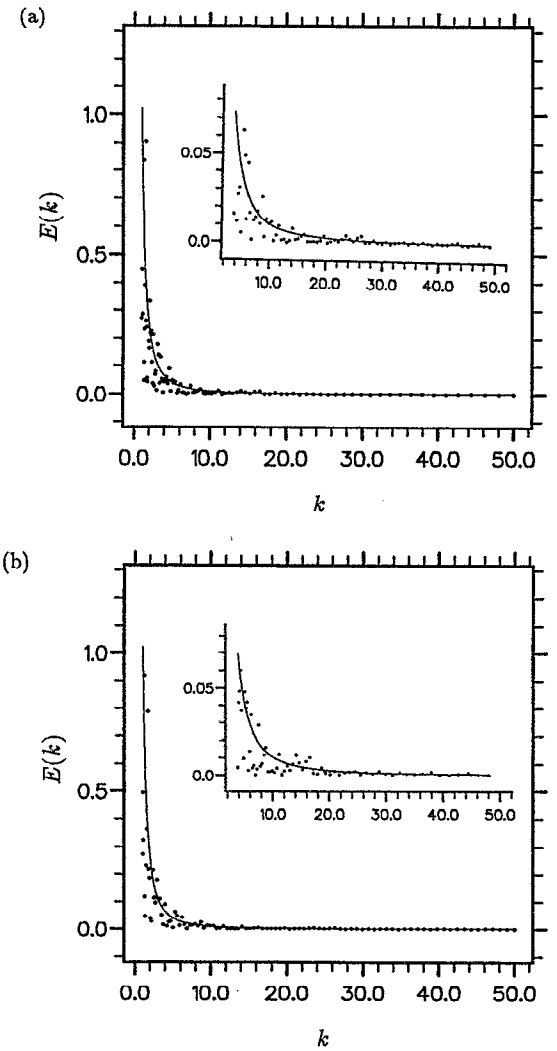

FIG. 2. The graphs show how imperceptible the difference is between the energy distributions at higher wavenumbers in (a) SGKS and (b) SAKS. The inserted plots are blown up energy spectra showing in more detail the distribution of energy where $E(k)<0.07$.

trajectories can be very complex if a time dependence is added to the flow (see Aref,[29] Ottino[10]). Here, we will make the cellular flow unsteady in two different ways: (i) by letting U_0 oscillate in time as follows:

$$U_0=U_0(t)=A[1+\mu\cos(\omega t)], \tag{27a}$$

where A is a constant magnitude, and where the unsteadiness of the flow field may be varied by varying either μ or ω, or (ii) by replacing the waves (26) with travelling waves, that is by replacing (26) with

$$u=U_0\sin\left(\frac{\pi x}{L}+\omega t\right)\cos\left(\frac{\pi y}{L}+\omega t\right), \tag{27b}$$

$$v=-U_0\cos\left(\frac{\pi x}{L}+\omega t\right)\sin\left(\frac{\pi y}{L}+\omega t\right), \tag{27c}$$

where the unsteadiness of the flow field may only be varied by varying ω.

This article is copyrighted as indicated in the article. Reuse of AIP content is subject to the terms at: http://scitation.aip.org/termsconditions. Downloaded to IP: 155.198.172.98 On: Fri, 12 Jun 2015 13:29:57

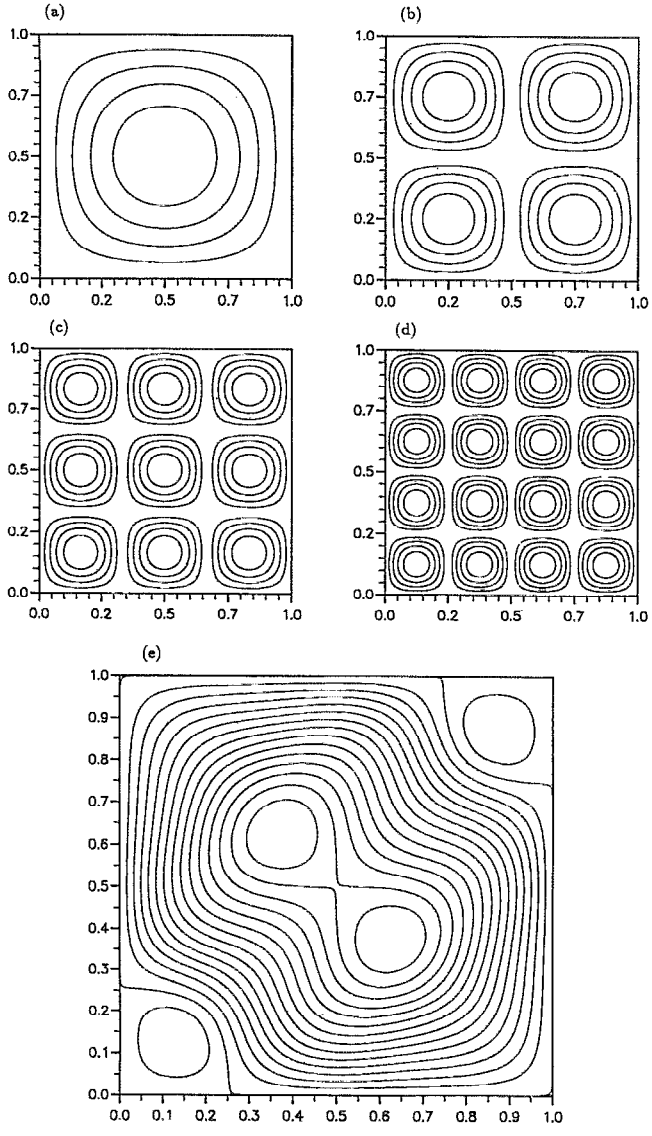

FIG. 3. The graphs show the streamlines for a periodic cellular flow field with one mode only but with different wavenumbers $k=1/L$ (a) $k=\pi$; (b) $k=2\pi$; (c) $k=3\pi$; (d) $k=4\pi$ and (e) a superposition of all previous four modes, i.e. $N_k=4$.

Note that such cellular velocity fields may be expressed in a form similar to Kinematic Simulation; for example, (26) and (27a) imply that

$$\begin{pmatrix} u \\ v \end{pmatrix} = \frac{A}{2}\begin{pmatrix} 1 \\ -1 \end{pmatrix}\sin\left(\frac{\pi x}{L}+\frac{\pi y}{L}\right)+\frac{A}{2}\begin{pmatrix} 1 \\ 1 \end{pmatrix}\sin\left(\frac{\pi x}{L}-\frac{\pi y}{L}\right)$$
$$+\frac{A}{2}\mu\begin{pmatrix} 1 \\ -1 \end{pmatrix}\sin\left(\frac{\pi x}{L}+\frac{\pi y}{L}+\omega t\right)$$
$$+\frac{A}{2}\mu\begin{pmatrix} 1 \\ 1 \end{pmatrix}\sin\left(\frac{\pi x}{L}-\frac{\pi y}{L}+\omega t\right)$$
$$+\frac{A}{2}\mu\begin{pmatrix} 1 \\ -1 \end{pmatrix}\sin\left(\frac{\pi x}{L}+\frac{\pi y}{L}-\omega t\right)$$
$$+\frac{A}{2}\mu\begin{pmatrix} 1 \\ 1 \end{pmatrix}\sin\left(\frac{\pi x}{L}-\frac{\pi y}{L}-\omega t\right). \tag{28}$$

In order to have a velocity field with more than one length scale, we generate superimposed cellular (SC) flows with different cell sizes; the SC1 flow is given by

$$u=\sum_{n=1}^{N_k} A_n[1+\mu\cos(\omega_n t)]\sin(k_n x)\cos(k_n y), \tag{29a}$$

$$v=-\sum_{n=1}^{N_k} A_n[1+\mu\cos(\omega_n t)]\cos(k_n x)\sin(k_n y), \tag{29b}$$

and the SC2 flow is

$$u=\sum_{n=1}^{N_k} A_n\sin(k_n x+\omega_n t)\cos(k_n y+\omega_n t), \tag{30a}$$

$$v=-\sum_{n=1}^{N_k} A_n\cos(k_n x+\omega_n t)\sin(k_n y+\omega_n t), \tag{30b}$$

where $\omega_n=\lambda k_n$, and $k_n=n\pi$. In the case of (29), the SC1 flow is *confined* in a control area of length and width equal to 1. It should also be noted that the SC1 and SC2 velocity fields are both periodic in time with period $T=2/\lambda$.

In the present simulations, the total number of modes is $N_k=4$, and $A_n=2/n$. Typical streamlines for a superposition of four periodic cellular flows are shown in Fig. 3e.

E. Summary of velocity fields

The number of modes, the range of wavenumbers and the choice of p, wavemode amplitudes, unsteadiness and distribution of wavemodes for different flow fields are summarised in Table I.

F. The release of a line in a turbulent-like flow: Resolution and integral length and time scales

Releasing a line in a flow is numerically equivalent to releasing a large sequence of points such that each two consecutive points of the sequence are at a very small initial resolving distance Δx apart. Given the flow field, and in particular its length scales and total kinetic energy per unit mass $E=E_\rho/\rho$, one has to choose the value of Δx subject to two restrictions:

(a) the initial distance between two points on the line has to be much smaller than the smallest scale of motion $2\pi/k_{N_k}$, i.e.

$$\Delta x \ll 2\pi/k_{N_k}; \tag{31}$$

(b) the initial distance between two points of the line must be significantly larger than the average distance travelled by a fluid element in one time step Δt (Δt is the resolution time step of the numerical integration), i.e.

$$\Delta x \gg \sqrt{2E}\Delta t. \tag{32}$$

(32) guarantees that the order of the sequence of points that constitutes the line is conserved, thus forbidding crossovers.

The time step Δt has to be smaller than all the time scales of the flow field. These time scales are the unsteadi-

This article is copyrighted as indicated in the article. Reuse of AIP content is subject to the terms at: http://scitation.aip.org/termsconditions. Downloaded to IP: 155.198.172.98 On: Fri, 12 Jun 2015 13:29:57

TABLE I. Summary of velocity fields.

	Form of velocity field	Number of modes N_k	Extreme wavenumbers k_1 and k_{N_k}	Value of p, where $E(k) \sim k^{-p}$	Wavemode amplitudes	Unsteadiness	Distribution of wavemodes
DKS	Eq. (15)	60	$k_1=1$ $k_{N_k}=100$	p=3.0, 3.2, 3,4 3.6, 3.8, 4.0	$\lvert U(k_n)\rvert \sim k_n^{-(1+p)/2}$	Eq. (20) $\omega_k \sim \lambda k^{(1-p)/2}$	Geometric Eq. (23)
SAKS	Eq. (15)	100	$k_1=1$ $k_{N_k}=100$	p=1.0, 1.67, 2.0, 3.0, 4.0	$U(k_n)$ drawn from a distribution of mean zero and variance given by Eq. (19)	Eq. (21) $\omega_k \sim \lambda k^{(3-p)/2}$	Algebraic Eq. (24a)
SGKS	Eq. (15)	100	$k_1=1$ $k_{N_k}=100$	p=1.0, 1.67, 2,0 3.0, 4.0		Eq. (21) $\omega_k \sim \lambda k^{(3-p)/2}$	Geometric Eq. (24b)
SC1	Eq. (29)	4	$k_1=\pi$ $k_{N_k}=4\pi$	N. A.	$A_n = 2/n$	$\omega_n = \lambda n\pi$	Algebraic/linear $k_n = n\pi$
SC2	Eq. (30)	4	$k_1=\pi$ $k_{N_k}=4\pi$	N.A.	$A_n = 2/n$	$\omega_n = \lambda n\pi$	Algebraic/linear $k_n = n\pi$

ness times $2\pi/\omega_k$, and the eddy turnover times $2\pi/\sqrt{k^3E(k)}$. In the SAKS and SGKS flows, $2\pi/\omega_k=2\pi/\sqrt{k^3E(k)}$, but in the DKS flows $2\pi/\omega_k=2\pi/\lambda kU(k)$ and is therefore different from $2\pi/\sqrt{k^3E(k)}$. Provided $p\geqslant 1$, $2\pi/\lambda kU(k)$ is bounded from below by $2\pi/(\lambda C)$ for all k $(1\leqslant k\leqslant 100)$, where $U(k)=Ck^{-(1+p)/2}$. The choice of the normalisation constant C is in fact a choice of total kinetic energy per unit mass E since –from (17)– $E=2\int_1^{100}kU^2(k)\,dk$. The normalisation constant also appears in $E(k)=2C^2k^{-p}$, and the eddy turnover time is $2\pi/\sqrt{k^3E(k)}=\sqrt{2}\pi k^{(p-3)/2}/C$ in the case of the DKS, SAKS and SGKS flows. The constant C may be calculated for all DKS, SAKS and SGKS flows on the basis of $E=\int_1^{100}2C^2k^{-p}\,dk$ which implies that

$$E\approx\frac{2C^2}{p-1} \tag{33a}$$

when p is significantly larger than 1 (as is the case for all the values of p used here that are different from 1), and

$$E=4C^2\ln 10 \tag{33b}$$

when $p=1$ (consider the limit $p\to 1$).

For the DKS flows with $p\geqslant 3$ there are, therefore, two constraints on Δt:

$$\Delta t\ll\frac{2\pi}{\lambda C}=\frac{2\pi}{\lambda}\left[\frac{2}{(p-1)E}\right]^{1/2} \tag{34a}$$

and

$$\Delta t\ll\frac{\sqrt{2}\pi}{C}=\sqrt{2}\pi\left[\frac{2}{(p-1)E}\right]^{1/2}. \tag{34b}$$

For the SAKS and SGKS flows with $p\geqslant 1$ there is only one constraint on Δt, namely

$$\Delta t\ll\frac{\sqrt{2}\pi}{C}k_{N_k}^{(p-3)/2}=\frac{\sqrt{2}\pi}{C}10^{p-3} \tag{35a}$$

if $p<3$, and

$$\Delta t\ll\frac{\sqrt{2}\pi}{C} \tag{35b}$$

if $p\geqslant 3$. Note that if (31) and (32) are satisfied, then so are (34b) and (35). Alternatively, if (34) or (35) is satisfied, then it is possible to find a resolution Δx that obeys (31) and (32).

The integral length scale L_T of a flow field is the decorrelation length of the velocity field, and is calculated as follows (L_T is Batchelor's[30] longitudinal integral length scale, and (36) can be rigorously deduced from Batchelor's[30] definition when the turbulence is 2-D and isotropic):

$$L_T=\int_1^{100}\frac{E(k)}{kE}\,dk, \tag{36}$$

where E is obtained by integrating $E(k)=2C^2k^{-p}$ between $k=1$ and $k=100$ in the case of SAKS, SGKS and DKS flows. Introducing (33) in (36) we obtain

$$L_T\approx(1-1/p) \tag{37a}$$

if p is significantly larger than 1, and

$$L_T=\frac{1}{2\ln 10} \tag{37b}$$

if $p=1$. L_T is always significantly smaller than $2\pi/k_1$.

The Lagrangian time scale of the velocity field is defined by

$$T_L=\frac{L_T}{\sqrt{2E}}. \tag{38}$$

$E=0.1$ in all DKS flows and $E=1.0$ in all SAKS and SGKS flows, and we adjust C according to (33) as we vary p. When p is varied between 5/3 and 4, L_T changes from 0.4 to 0.75 and T_L varies between 0.92 and 1.72 for the SAKS and SGKS flows. We vary p between 3 and 4 in the DKS and L_T and T_L vary, respectively, between 0.66 and 0.75 and between 0.3 and 0.52. When $p=1$ (SAKS and SGKS flows), $L_T\approx 0.2$ and $T_L\approx 0.4$. Thus, the integral length and time

This article is copyrighted as indicated in the article. Reuse of AIP content is subject to the terms at: http://scitation.aip.org/termsconditions. Downloaded to IP: 155.198.172.98 On: Fri, 12 Jun 2015 13:29:57

scales have roughly the same order of magnitude in all our numerical experiments involving a KS flow (SAKS, SGKS and DKS).

The relevant integral length and time scales of the SC1 and SC2 velocity fields are the size of the square cell $L_C=2\pi/k_1=2$ and the Lagrangian time scale is defined by $T_L=L_C/\sqrt{2E}$. In our SC1 and SC2 flows, $E\approx 1.04$ and therefore $T_L\approx 1.4$. The time step Δt must be significantly smaller than both $(A_n k_n)^{-1}$ and ω_n^{-1}. Thus, for SC1 and SC2 flows, the constraint on the choice of Δt is

$$\Delta t \ll \frac{1}{2\pi}\inf\left(1,\frac{1}{2\lambda}\right). \tag{39}$$

If (39) is satisfied, then it is possible to find a resolution Δx that obeys (31) and (32).

The fluid element trajectories are computed with a standard predictor–corrector scheme (Hamming[31]) or an adaptive stepsize control for fourth-order Runge–Kutta (Press *et al.*[32]). For the predictor–corrector schemes, our time steps Δt vary between 10^{-2} and 10^{-5} (10^{-2} in the SC flows, 0.005 in the SAKS and SGKS flows, and between 10^{-3} and 10^{-5} in the DKS flows). We checked that smaller time steps do not give significantly better accuracy. The adaptive stepsize control method automatically chooses the stepsize so as to achieve a predetermined accuracy in the solution with minimum computational effect. Δt is always small enough to guarantee (34), (35) or (39) (depending on which flow we run). The resolution distance Δx can then be chosen under the constraints (31) and (32). The choice of Δx is a choice of the initial length L_0 and of the number N of points on the line; $\Delta x=L_0/N$.

In the DKS flows, we always take at least 1000 points on lines for each run (often we take 2000). The initial length L_0 of the lines we release varies between 0.08 and 1, and so the initial separation Δx varies between orders of magnitude 10^{-3} and 10^{-5}. (L_0 is small, e.g. $L_0=0.08$, when we release the line in specific eddy regions of the DKS flow; when L_0 is order 1, it is comparable to L_T because $0.66\leqslant L_T\leqslant 0.75$ in our DKS flows where $3\leqslant p\leqslant 4$.) In the SAKS and SGKS flows, $N=15\,000$ and $L_0=0.1$ when $p=1$ ($L_T=0.2$), and $\Delta x=6.6\times 10^{-6}$. However $L_0=1$ and N is equal to either 15 000 or 20 000 for all other values of p ($0.4\leqslant L_T\leqslant 0.75$), in which case Δx is either 6.6×10^{-5} or 5×10^{-6}. Finally, in the SC1 and SC2 flows, $N=30\,000$, $L_0=1$ ($L_C=2$) and $\Delta x=3.3\times 10^{-5}$.

G. The geometrical scaling exponents D_K and D

To calculate the Kolmogorov capacity D_K we should cover the line with the minimum number of boxes of a given size. It is of course impractical to find such a minimum numerically. Instead, we set a grid of square cells of side length ϵ on the plane of the flow where the line is advected, and we count how many of these cells contain at least one of the points that constitute the numerical implementation of the line. Such a procedure is standard (see Mandelbrot[33]) and is shown in Falconer[25] to be equivalent to the most economical covering in the limit of vanishingly small boxes ($\epsilon\to 0$). For boxes of intermediate size such as are used in practice it gives accurate answers. The Kolmogorov capacity D_K exists if $N(\epsilon)$ has a power law dependence on ϵ, in which case

$$D_K=-\frac{\log N(\epsilon)}{\log\epsilon}. \tag{40}$$

The algorithm was applied to various curves of known Kolmogorov capacity (e.g. the Koch curve) and a numerical value for these capacities was obtained that is in very good agreement with the known value. The range of values of ϵ where we investigate the existence of a Kolmogorov capacity is $1/k_{N_k}=0.01\leqslant\epsilon\leqslant 0.1$ in the DKS flow, and $2\pi/100k_{N_k}\leqslant\epsilon\leqslant 2\pi/k_{N_k}$ in all the other flows. It is well known that turbulence can generate scalar fluctuations, and thereby interfacial contortions, at scales much smaller than the Kolmogorov scale (Batchelor[34]). It is therefore not unreasonable to expect a non-trivial interfacial Kolmogorov capacity at scales below $2\pi/k_{N_k}$ as well as at scales above $1/k_{N_k}$.

We also look for a similarity law relating the line's length $L(t)$ at time t to a variable *initial* resolution $\epsilon_0=L_0/N_0$ of the line. When $N_0=N$, $\epsilon_0=\Delta x$. We vary N_0 between N and $N/25$, which means that we vary ϵ_0 between Δx and $25\Delta x$. A similarity law defines the dimension D introduced by Fung and Vassilicos[10] as follows:

$$L(\epsilon_0,t)\sim\epsilon_0^{1-D}. \tag{41}$$

The dimension D is computed by measuring the length $L(t)$ of the line at regular time intervals and for different initial resolutions ϵ_0, that is different numbers N_0 of points on the line. Fung and Vassilicos[10] conjectured that $D>1$ implies an H-fractal scaling topology; their conjecture is now proved in the present paper's Appendix under the assumption that no isolated regions exist where the flow velocity if either unbounded or undefined in finite time. It is also proved in the Appendix that $D_H>1$ implies $D>1$ under no assumptions. As emphasized by Fung and Vassilicos[10] though, the relation between D_H and D remains unknown. Fung and Vassilicos[10] found $D>1$ for lines advected by Aref's[29] blinking vortex, and $D=1$ for a line advected by a steady vortex. However, $D_K>1$ in both the steady and the blinking vortices. We can now safely conclude that a line in an *unsteady 'blinking'* vortex becomes H-fractal, whereas a line in a *steady* vortex becomes K-fractal (in fact, spiral).

The simulations done here are very expensive because of the box-counting algorithm (e.g.: see Giorgilli *et al.*[35] for a brief discussion of its numerical cost). In the sequel we measure the advected line's D and D_K as functions of time, which means that we use the box-counting algorithm at regular time intervals during the evolution of the line. Thus, our calculations are very time consuming, and our study would have been out of reach if other velocity fields were used, such as a DNS (Direct Numerical Simulation) turbulent flow for example. A DNS turbulent flow requires the calculation of the velocity field at each time step over the entire domain and has only a limited range of self-similar scales. Kinematic Simulation and SC flow velocities need only be calculated at the interface, and the range of self-similar scales of motion can be prescribed at will to be comparatively very large.

This article is copyrighted as indicated in the article. Reuse of AIP content is subject to the terms at: http://scitation.aip.org/termsconditions. Downloaded to IP: 155.198.172.98 On: Fri, 12 Jun 2015 13:29:57

III. THE SCALING TOPOLOGIES OF LINES ADVECTED BY 2-D TURBULENT-LIKE FLOWS

A. The time invariance of topological scaling exponents in single flow realisations

In the theory of turbulence, the concept of a steady state is traditionally used in the statistical sense. The statistics over many realisations of a homogeneous and isotropic equilibrium turbulence are assumed to be independent of time (Kolmogorov[36]), and so are the statistics of a scalar passively advected by such a turbulence (Batchelor[34]). But does the topology of a turbulent interface reach a steady state in a *specific realisation* of the turbulence, even though the flow continues to advect, stretch and bend the interface? And is it absolutely necessary that the interface be space-filling when it reaches the steady state?

Here we address the specific question whether the geometrical scaling exponents D_K and D of a continuously evolving interface exist, are non-trivial and reach an asymptotic non-space-filling steady state in specific realisations of a turbulent-like flow. This question is not a trivial one. A passive scalar F in a turbulent flow field has the property that $\overline{|\nabla F|^2}$ increases indefinitely with time when its diffusivity is zero. Batchelor[37] has shown this property to be a consequence of the exponential increase of the area of isoscalar surfaces, and therefore of their increased folding or roughness. Such a mechanism could be consistent with an indefinite increase of the Kolmogorov capacity D_K of isoscalar surfaces towards space-fillingness, i.e. $D_K=d$ for $t\to\infty$ (d is the Euclidian dimension of the embedding space, here $d=2$). On the other hand, the property that $\overline{|\nabla F|^2}\to\infty$ as $t\to\infty$ may also be consistent with the growth of smaller and smaller scales of wrinkles (a cascade) on the interface in a steady self-similar way, in which case the interface may not become space-filling and the Kolmogorov capacity may have a single steady value over a growing range of length scales.

We initiate the present study by investigating numerically whether interfacial steady self-similar states exist. It is found that in *all* the 2-D turbulent-like flows generated here, the advected lines have non-trivial Kolmogorov capacities which reach an asymptotically constant value in time that is smaller than the space-filling value 2. Surprisingly, this property holds not only for steady but also for unsteady turbulent-like velocity fields. It is also found that D is always well-defined and asymptotically constant. However, D is non-trivial ($D>1$) only where the flows are unsteady.

We release initially straight lines of initial length L_0 equal to one integral length scale in all the DKS, SAKS and SGKS flows generated here. We generate DKS flows with six different self-similar energy spectra, that is six different values of the exponent p between 3 and 4, and SAKS and SGKS flows with exponents p equal to 1, 1.67, 2, 3, and 4. The lines very quickly (after about half a Lagrangian time scale) develop spiral singularities (see Fig. 4) which are sustained and accentuated as time progresses even when the velocity field is unsteady. Other topological features appear on the line, such as folds arising from a possible stretch and fold mechanism, particularly when the flow is unsteady (see Fig. 5).

The lines have well-defined Kolmogorov capacities in all cases at all times, that is, a relation of the type $N(\epsilon)\sim\epsilon^{-D_K}$ does hold in the ranges of length scales (box sizes) investigated. The slopes in the $\log N(\epsilon)$ – $\log\epsilon$ plots (see Fig. 6) steepen briefly until they stabilize to a steady fall-off after approximately one to half a Lagrangian time scale (in all the KS flows), and the capacity D_K remains constant thereafter (see Fig. 7).

An asymptotic steady state behaviour is also observed on the dimension D; a relation of the type $L(\epsilon_0,t)\sim\epsilon_0^{1-D}$ holds surprisingly well over a wide range of initial resolutions ϵ_0 (see Fig. 8), and D asymptotes to a constant value D after approximately two Lagrangian time scales in all the KS flows (see Fig. 9). The dimension D has been computed at regular intervals of time in all our flows except the DKS flows. It is found that $D=1$ in the steady velocity fields, and that $D>1$ in the unsteady velocity fields.

The same experiments are done with the SC1 and SC2 flows, and similar conclusions on the Kolmogorov capacities D_K and the dimensions D are reached (Figs. 10, 11 and 12). However, D_K and D reach their asymptotic state in, respectively, approximately 7 and 15 Lagrangian time scales ($T_L\approx 1.4$ in the SC flows). The time it takes the dimensions D_K and D to converge to their constant asymptotic value is greater when the number of modes of the flow is smaller ($N_k=O(1)$ in the SC flows, and $N_k=O(10^2)$ in the KS flows). Also, note that D always takes longer than D_K to converge.

Finally, we observe that the scaling properties of line-interfaces react very differently to the onset of flow unsteadiness according to whether they are embedded in a SC1 or a SC2 flow.

B. The effect of flow unsteadiness on the scaling steady state

We have run two different versions of each DKS flow generated here, one steady [$\lambda=0$ in (20)] and one unsteady [$\lambda=1$ in (20)]. In the cases $p=1$, $p=2$ and $p=3$, the SAKS and SGKS flows were run for four different values of λ in (21): $\lambda=0.0,0.2,0.4,0.6$. With one notable exception, the capacity D_K is usually larger when the KS flows are steady rather than unsteady, and appears to be a decreasing function of unsteadiness, i.e. $dD_K(\lambda)/d\lambda<0$ (see Fig. 13). It is interesting to note that, in the DKS flows considered here, the unsteadiness frequency ω_k is a decreasing function of wavenumber k [see (20)], whereas ω_k is a non-decreasing function of k in the SAKS and SGKS flows where $p\leqslant 3$ [see (21)]. Nevertheless, D_K is in general a decreasing function of λ in both DKS and SAKS/SGKS flows. The exception is the SAKS flow with $p=2$, where D_K does not exhibit a downwards trend with increasing λ. The reason for this different behaviour is not yet clear. Some insight is reached in our discussion of the difference between algebraic and geometric progressions of wavenumbers in section III.F.

The KS flows have a large number of degrees of freedom in the sense that N_k is large ($N_k=60$ in DKS, $N_k=100$ in SAKS and SGKS). On the contrary, the SC flows have a small number of degrees of freedom ($N_k=4$), and the effect of unsteadiness on D_K is quite different. We find that

This article is copyrighted as indicated in the article. Reuse of AIP content is subject to the terms at: http://scitation.aip.org/termsconditions. Downloaded to IP: 155.198.172.98 On: Fri, 12 Jun 2015 13:29:57

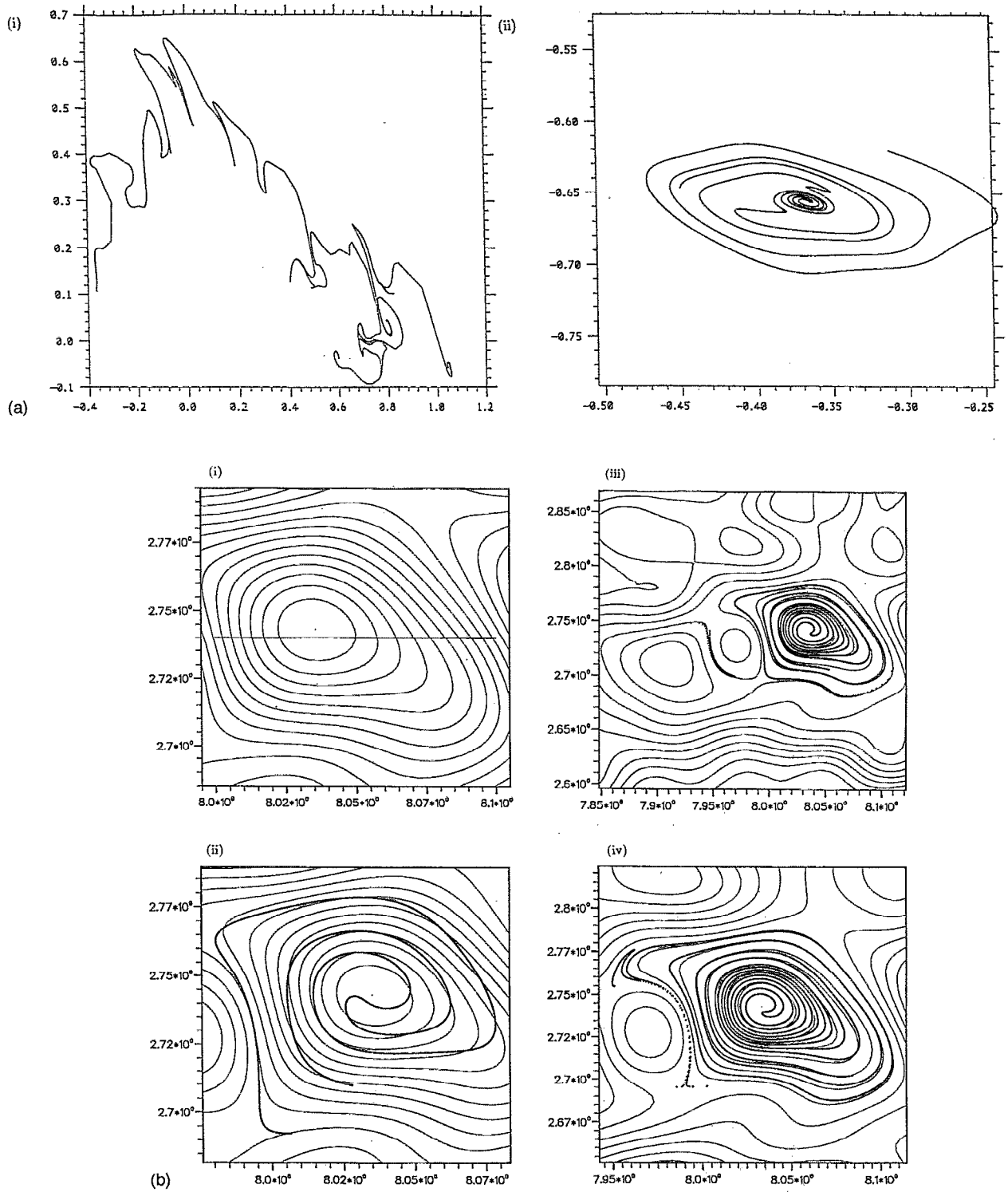

FIG. 4. (a) (i) Line in a DKS flow field at time $t=0.7T_L$. The line was initially straight with coordinates $y=-0.1$ and x between 0.0 and 1.0. The integral length scale is $L_T \approx 1$. 2000 points constitute the line. (ii) Line released initially straight and 1/12 long in an eddy region of a DKS flow, having developed a spiral structure. The integral length scale is $L_T \approx 1$ and $t=2.5T_E$. The flow is steady. (b) The graphs show example of a spiral generated from a straight line of initial length 1 (20 000 points constitute the line) in a SAKS flow at different times (i) $t=0.0$; (ii) $t=0.2$; (iii) $t=0.65$ and (iv) $t=0.85$. The flow is steady, i.e. $\lambda=0.0$ and the other parameters are $N_k=100$, $p=1$, $k_1=1$ and $k_{N_k}=100$. (c) The graphs show examples of spirals and tendrils generated from a straight line of initial length 1 (20 000 points constitute the line) in a SAKS flow at different times (i) $t=0.0$; (ii) $t=0.2$; (iii) $t=0.65$ and (iv) $t=0.85$. The flow is *unsteady* with $\lambda=0.2$ and the other parameters are $N_k=100$, $p=1$, $k_1=1$ and $k_{N_k}=100$. (Note: only the SAKS flows are shown here but similar features can be observed in SGKS flows.)

This article is copyrighted as indicated in the article. Reuse of AIP content is subject to the terms at: http://scitation.aip.org/termsconditions. Downloaded to IP: 155.198.172.98 On: Fri, 12 Jun 2015 13:29:57

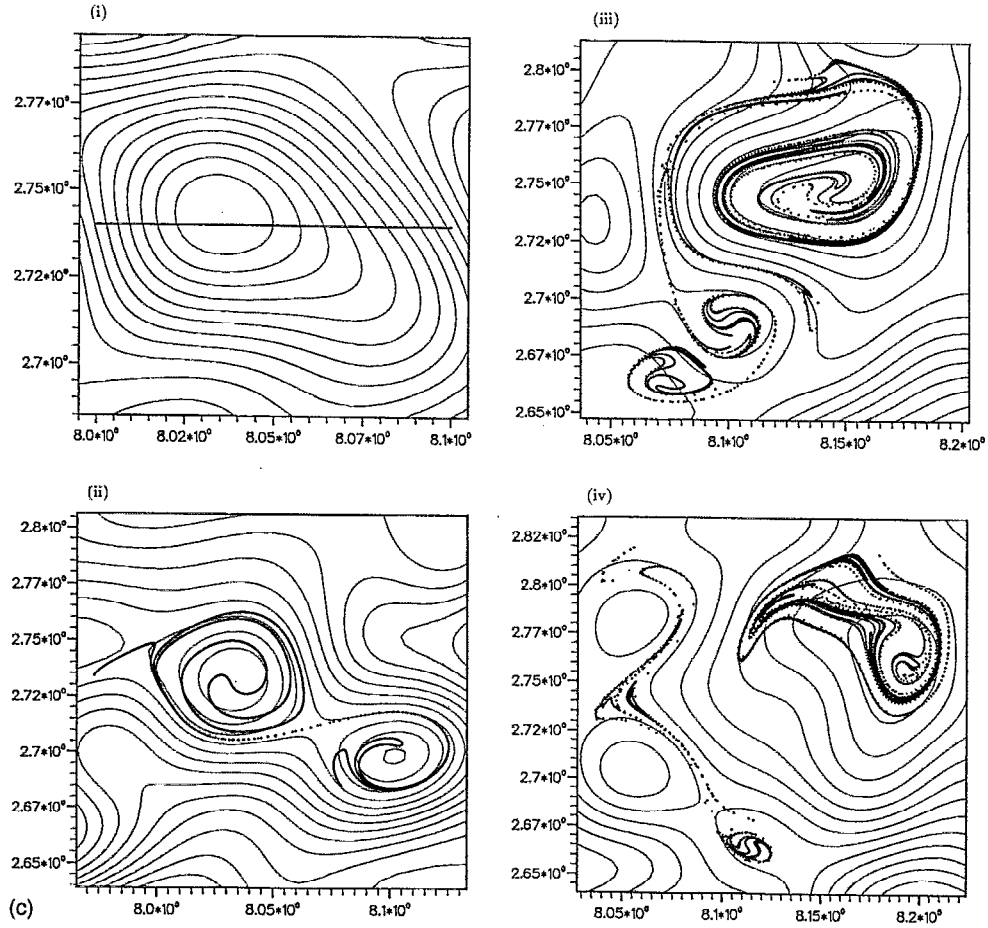

FIG. 4. (*Continued.*)

D_K is an *increasing* function of both λ and μ [see Figs. 14(a) and (b)] in the SC1 flows. However, in the SC2 flows, D_K first decreases with increasing λ when λ is very small, and then increases with increasing unsteadiness at the larger values of λ (see Fig. 14c).

The dimension D is found to be an increasing function of unsteadiness in all the tested flows (see Table II); D is an increasing function of both μ and λ in the SC1 flows [see Figs. 15(a) and (b)], an increasing function of λ is the SC2 flows (see Fig. 15c) and an increasing function of λ in the SAKS and SGKS flows mentioned in the previous paragraph (Fig. 16). However, $D-1$ remains small in the KS flows where N_k is large, and grows to values below but close to 1 in the SC flows where N_k is small.

We now attempt to understand some of the scaling properties of the lines advected by our turbulent-like velocity fields in terms of the topologies of the flows.

C. The relation between the interfacial scaling exponents D_K and D and the topology of the flow

The instantaneous streamline pattern of a 2-D incompressible flow is essentially made of three different topological types of regions (see for example Wray and Hunt,[7] Fung *et al.*[19] and Hunt *et al.*[38]): the eddy regions which are strong swirling regions with vorticity, the convergence regions surrounding a saddle point where there is irrotational straining (in these regions there is 'convergence' of streamlines) and the streaming regions where the flow is very weakly curved and runs rather fast (see Fig. 1). Berry *et al.*[8] have made a first attempt to classify the convolutions of curves in phase planes evolving under the action of continuous area-preserving *maps*. They point out that the complexity of such curves is totally due to the fixed points of the map. These are the elliptic and the hyperbolic fixed points whose analogues in the instantaneous streamline pattern of fluid flows are respectively the eddy and the convergence regions. Berry *et al.*[8] argue that the only contortions that the line can develop are either 'whorls' (spirals) when the curve passes through—or near—an elliptic point, or 'tendrils' when it passes through —or near—a hyperbolic point. In that same spirit, we find that lines in the present 2D turbulent-like flows are spiral in the eddy regions, but not in the other regions. This result holds irrespective of whether the flow is time-dependent or not, but provided that the unsteadiness of the flow is not too violent so that eddy streamline structures may remain in the same approximate region of space for long enough times.

We release straight lines of small initial length (typically smaller than one tenth of the integral length scale of the turbulence) into specific regions of a DKS flow. The object

This article is copyrighted as indicated in the article. Reuse of AIP content is subject to the terms at: http://scitation.aip.org/termsconditions. Downloaded to IP: 155.198.172.98 On: Fri, 12 Jun 2015 13:29:57

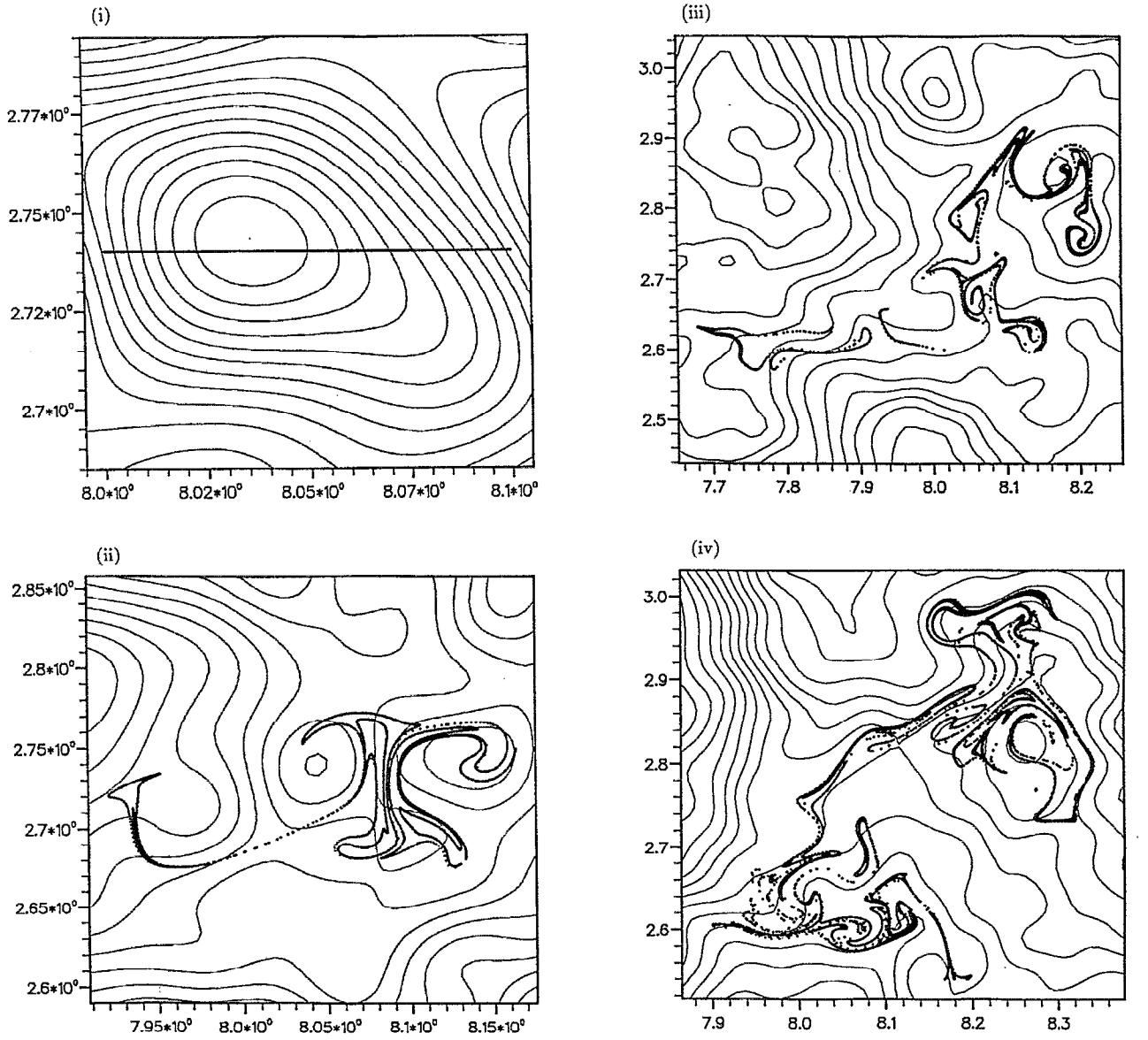

FIG. 5. As the unsteadiness parameter λ increases (here in a SAKS flow), topological features other than spirals appear on the line (initially straight with length 1; 20 000 points constitute the line), such as tendrils (folds) arising from a possible stretch and fold mechanism. Examples of folds generated in a SAKS flow with $\lambda=0.4$ are shown at different times (i) $t=0.0$; (ii) $t=0.275$; (iii) $t=0.55$ and (iv) $t=0.75$. The other parameters are $N_k=100$, $p=1$, $k_1=1$ and $k_{N_k}=100$. Note the coexistence of tendrils and spirals and the evolution in time of their relative importance (simliar features can also be observed in SGKS flows).

of the exercise is to detect regions of the flow where the capacity D_K of the line exceeds 1, and the geometrical patterns this excess is related to.

One might naively think that a non-integer value of D_K is always linked to a fast line growth. But that does not necessarily hold. In the convergence regions, where there is high straining, and where the line growth is exponential, the line simply stretches and remains fairly straight (Fig. 17) so that $D_K=1$. On the contrary, in the eddy regions the line develops a spiral topology (see Fig. 4), as a consequence of which $D_K>1$ (Fig. 7a), even though the line growth there is only linear (Fig. 18). The larger the value of D_K, the slower the winding of the spiral onto its centre (see Vassilicos and Hunt[6]).

These numerical experiments are done for both steady and unsteady DKS velocity fields. The conclusions are the same in both cases and are summarised in Table III.

In general, these spirals are not the only interfacial topological feature responsible for the non-integer value of the interface's D_K. Tendrils may also contribute to the value of D_K, and indeed, we do observe tendrils, but only in the unsteady flow simulations. Furthermore, in all the DKS, SGKS and SAKS flows used here, D_K is not an increasing function of the unsteadiness parameter λ. In fact, with the sole exception of SAKS with $p=2$, D_K is a *decreasing* function of unsteadiness. It may be expected that when λ is not too large, the only, or at least, the predominant mechanism by which lines acquire a non-integral D_K is their winding

This article is copyrighted as indicated in the article. Reuse of AIP content is subject to the terms at: http://scitation.aip.org/termsconditions. Downloaded to IP: 155.198.172.98 On: Fri, 12 Jun 2015 13:29:57

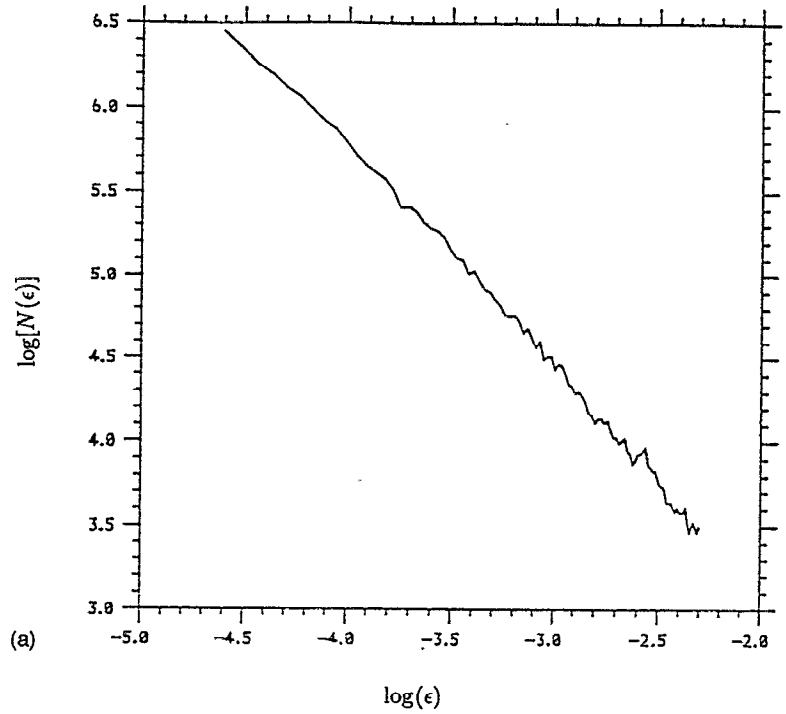

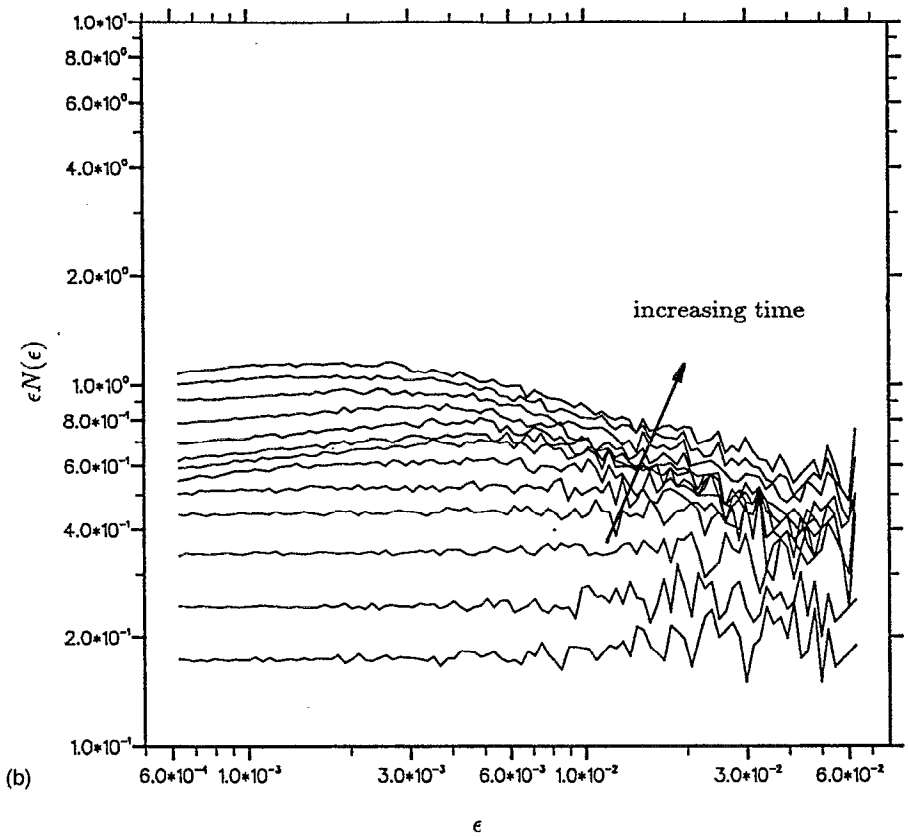

FIG. 6. (a) Typical example of a log−log plot (note: log is the natural logarithm) of $N(\epsilon)$ vs. ϵ for a line in a DKS flow. The range of values of ϵ is $0.01 \leqslant \epsilon \leqslant 0.1$. (b) The graph shows a log−log plot of $\epsilon N(\epsilon)$ vs. ϵ [since the slope is sometimes only slightly greater than 1, we plot $\epsilon N(\epsilon)$ vs. ϵ, so that the line is horizontal at $t=0$] in SGKS (the parameters are $N_k=100$, $p=1$, $k_1=1$ and $k_{N_k}=100$). As the time increases, the slope increases too until it reaches a constant slope of 0.4 at $t=0.325$ which is about half the Lagrangian time scale. (c) The caption is identical to Fig. 6b but for SAKS.

This article is copyrighted as indicated in the article. Reuse of AIP content is subject to the terms at: http://scitation.aip.org/termsconditions. Downloaded to IP: 155.198.172.98 On: Fri, 12 Jun 2015 13:29:57

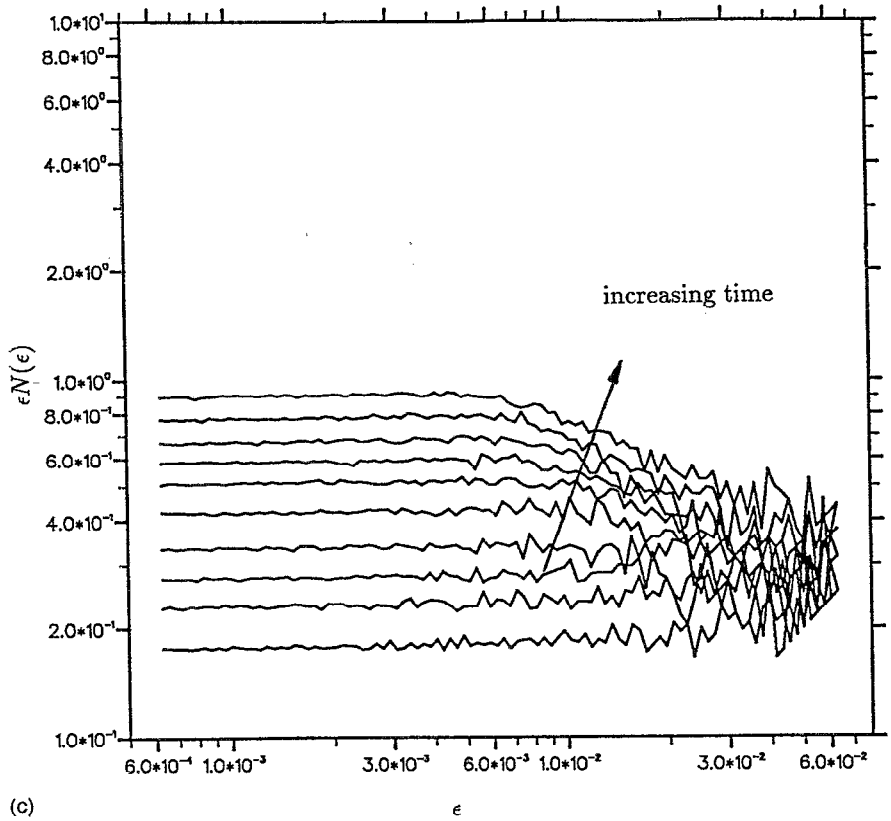

FIG. 6. (*Continued.*)

into spiral structures by eddy regions. Since eddy regions wobble about when the turbulence is unsteady, the decrease of D_K with increasing λ may be the result of the increasing loss of persistence of the eddy's windings of the line.

The dimension D increases with λ in all our flows. In the case of the SC1 flows where the unsteadiness is defined by two parameters λ and μ, D increases with both λ and μ. However, $D=1$ when the 2-D flows are steady. Line-interfaces are therefore K-fractal [provided no isolated regions exist where the flow velocity is either unbounded or undefined in finite time (see the Appendix), as is indeed the case in all the velocity fields here] in 2-D steady flows, and their non-integer Kolmogorov capacity only reflects the localised self-similar structure of spirals in the eddy regions. The fact that $D>1$ when the flows are unsteady indicates an H-fractal interfacial topology (see the Appendix), and the increase of D with increasing unsteadiness may signify an 'increased H-fractal topology' in a sense that is not yet absolutely clear. As the flow is made more unsteady, a mechanism different from the one where eddies generate interfacial spirals sets in and becomes gradually more important in determining the values of D_K and D. This different mechanism generates an H-fractal topology and may be the mechanism described by Berry *et al.*[8] where a line near a hyperbolic point undergoes a stretch and fold action because of the infinity of homoclinic and heteroclinic intersections between stable and unstable manifolds of hyperbolic points. In a two-dimensional stationary incompressible flow, there are no homoclinic and heteroclinic points other than the hyperbolic fixed points themselves, and the behaviour of the stable and unstable manifolds is not at all chaotic. So, following Berry *et al.*,[8] we should not expect to observe tendrils in 2-D steady flows. This stretch and fold mechanism—we may also call it a 'chaotic mechanism'—generates H-fractal tendrils on the interface. We do observe tendrils when the flows are unsteady and particularly when D is large (see Figs. 4, 5 and 10). We are led to conjecture that when $D-1$ is a small number then the value of D_K is dominated by the spiral aspect of the interfacial topology, even though $D>1$ implies that the line is H-fractal. For larger values of $D-1$ though, D_K reflects the scaling properties of the H-fractal topology of the interface, and therefore its chaotic tendril-like structure.

The spiral mechanism provides some insight into why D_K decreases with λ, but only for small values of λ. It remains unclear why D_K continues to decrease with λ even at relatively large values of λ in all the DKS, SGKS and SAKS (except when $p=2$) flows. In order to gain some further insight on the mechanisms by which unsteadiness modifies D_K, we release line-interfaces in the simpler SC1 and SC2 flows.

The SC1 flow is constructed in such a way that the unsteady jitter of eddies is confined within a limited region of space surrounded by streamlines that do not move but are frozen with respect to a fixed frame of reference. The square cells of size 1 have hyperbolic points at their four corners and their four sides are steady and unsteady manifolds linking these hyperbolic points together. These four manifolds are particular streamlines that do not move with time even

This article is copyrighted as indicated in the article. Reuse of AIP content is subject to the terms at: http://scitation.aip.org/termsconditions. Downloaded to IP: 155.198.172.98 On: Fri, 12 Jun 2015 13:29:57

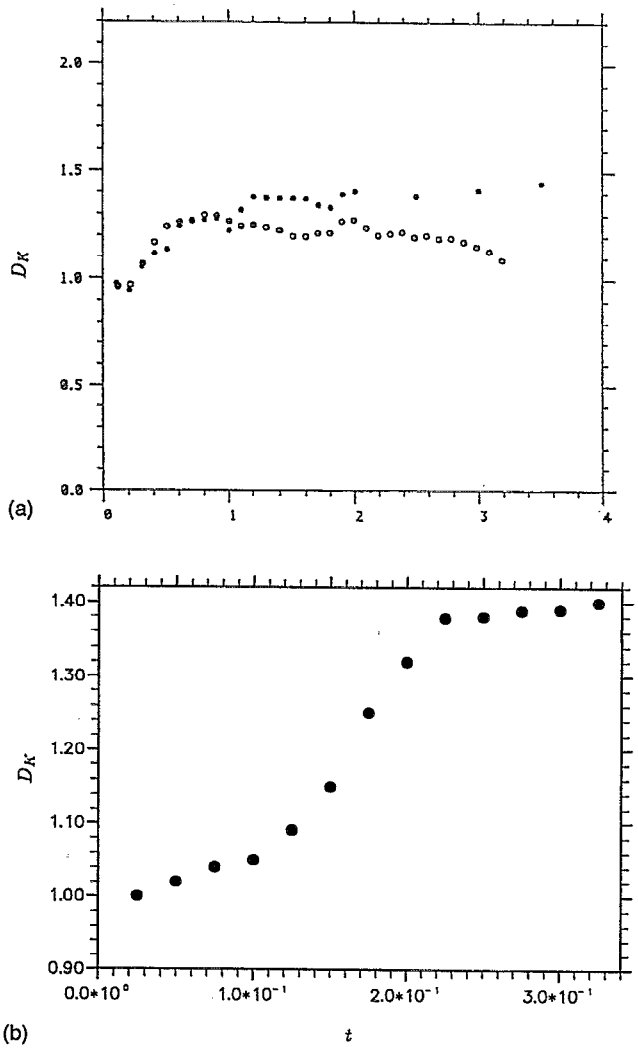

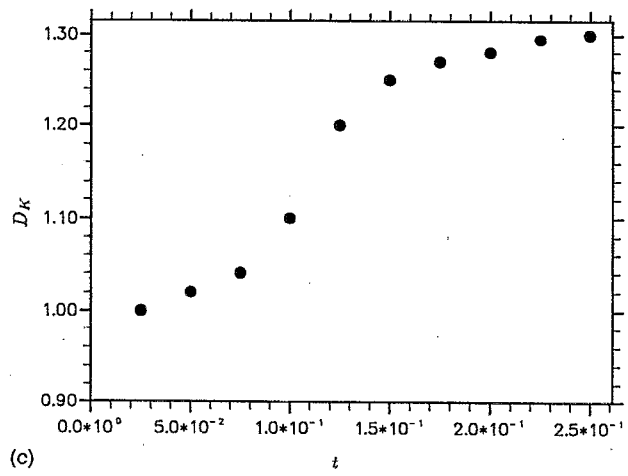

FIG. 7. (a) Capacity D_K of a line in an eddy region of a DKS flow field as a function of time. The time unit is $T_L=1$. *** frozen velocity field. OOO unsteady velocity field. (b) The capacity D_K of a line in a SGKS flow field as a function of time. D_K reaches a constant value of about 1.4 after about half a Lagrangian time scale. The other parameters are the same as in Fig. 6b and the capacity is obtained from the slopes of the lines of Figure 6b. (c) The capacity D_K of a line in a SAKS flow field as a function of time. D_K reaches a constant value of about 1.3 after about half a Lagrangian time scale. The other parameters are the same as in Fig. 6c and the capacity is obtained from the slopes of the lines of Figure 6c.

though the flow within the cell does vary with time. Surprisingly, D_K increases with both μ and λ in the case of SC1 flows (see Figs. 14 and 15). The confinement by immovable streamlines generates spirals on the line with a slower rate of inward convergence. The loss of persistence of the eddies' winding action which causes D_K to decrease with increasing unsteadiness seems to be offset in the SC1 flow by the confinement of the flow. The role of flow confinement in amplifying the interface's D_K may also be realised with solid boundaries. It would be interesting, for example, to study the topology of line interfaces in a blinking vortex (Aref[29]) confined within a circular solid boundary. Fung and Vassilicos[10] studied the dependence of D_K on the switching period of the blinking vortex *without* solid boundaries, and found that D_K increases with the switching period. It should be noted, however, that a line in Aref's[29] blinking vortex does not grow spirals but tendrils; since we do not yet understand how flow unsteadiness affects the Kolmogorov capacity D_K of H-fractal tendril interfaces, the effect of boundary confinement on the D_K of an interface advected by a chaotic flow is not trivial either. We leave this question for future work on the self-similar topology of passive interfaces advected by 2-D chaotic flows.

In order to test even further the spiral mechanism and its dependence on the persistence and confinement of eddies, we release lines in the SC2 flow which has no fixed cells in space. The SC2 unsteady flows are constructed in such a way that their entire cell structure deforms and oscillates in space. As may be expected from the lack of flow confinement in SC2 flows and the loss of persistence in the winding action of eddies, it is found that D_K decreases with λ but only for $\lambda \leqslant 0.1$. However, when $\lambda \geqslant 0.1$, D_K increases with λ, thus signalling the onset of a different mechanism. The topology of the interface is indeed dominated by spirals when $\lambda < 0.1$ but by tendrils when $\lambda > 0.1$ (see Fig. 10d). The mechanism that sets in when λ grows significantly larger than 0.1 may be the chaotic mechanism that generates H-fractal tendrils. Note that D has also grown significantly larger than 1.0 when $\lambda > 0.1$. It is not clear why the chaotic mechanism is such that $dD_K/d\lambda > 0$, but note that the same happens in Aref's[29] blinking vortex (chaotic advection) where tendrils dominate the interface's topology and D_K increases with increasing unsteadiness too (Fung and Vassilicos[10]).

The relation between stretching and D_K summarised in Table IV may have an interesting consequence for mixing in

This article is copyrighted as indicated in the article. Reuse of AIP content is subject to the terms at: http://scitation.aip.org/termsconditions. Downloaded to IP: 155.198.172.98 On: Fri, 12 Jun 2015 13:29:57

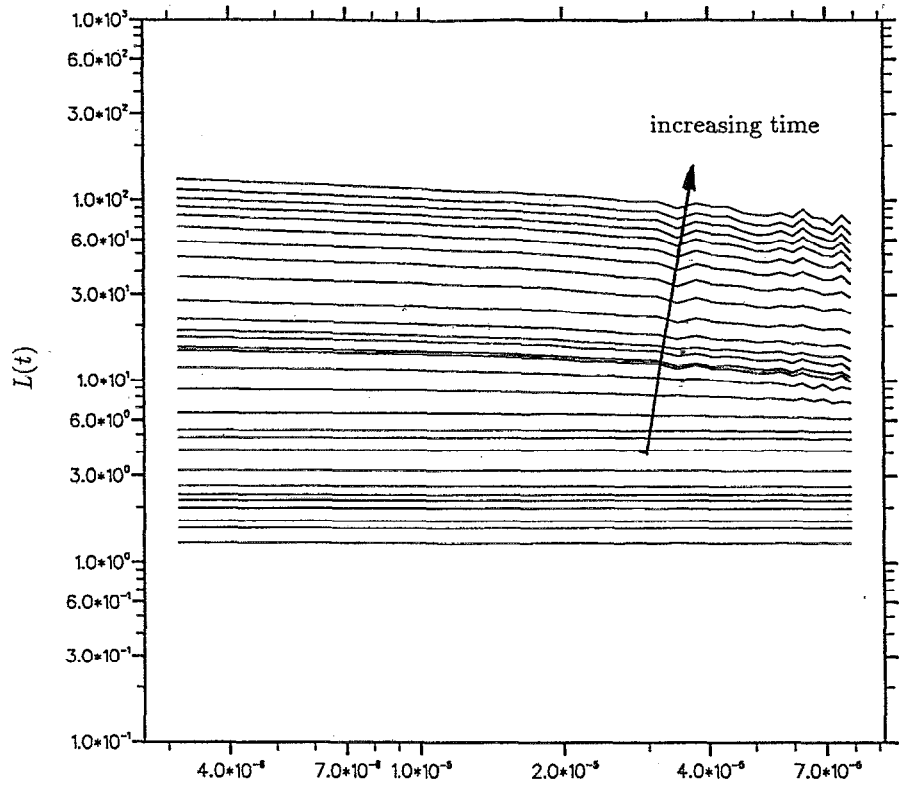

(a)

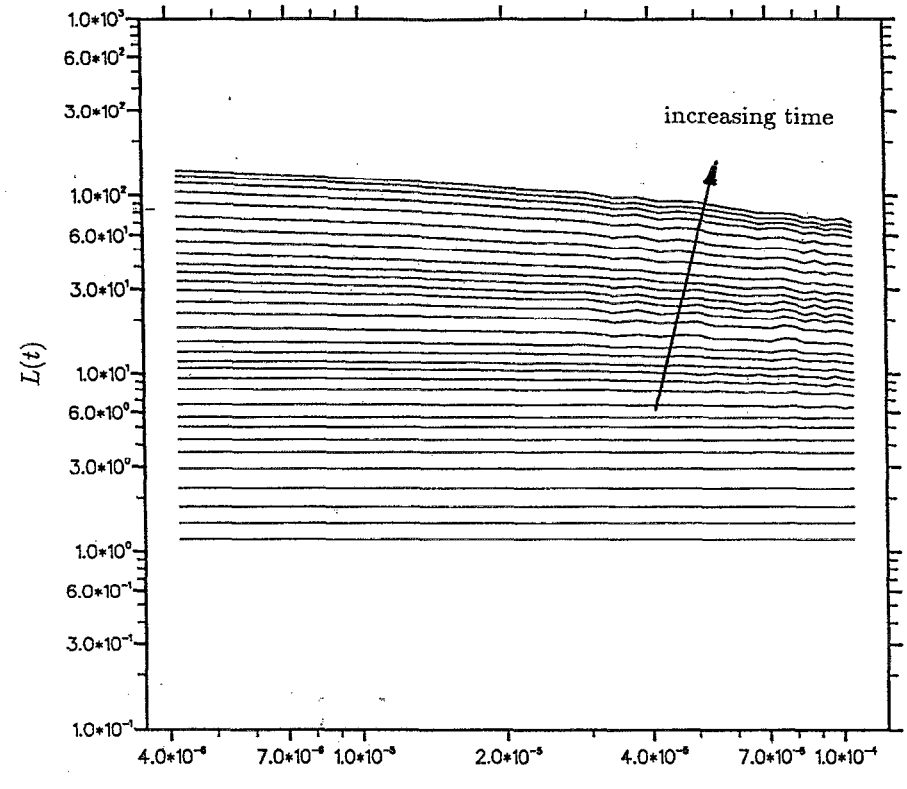

(b)

FIG. 8. (a) The graph shows $L(t)$ versus resolution (1/No. of points on the line) on a log−log plot and for a succession of times. The line is evolving in a SGKS flow, and the parameters are $N_k=100$, $p=2$, $k_1=1$ and $k_{N_k}=100$. Note that as time increases, so does the slope and the slope reaches an asymptotic value of 0.4. (b) The caption is identical to the one of Fig. 8a but for SAKS and the asymptotic value of the slope is 0.22.

This article is copyrighted as indicated in the article. Reuse of AIP content is subject to the terms at: http://scitation.aip.org/termsconditions. Downloaded to IP: 155.198.172.98 On: Fri, 12 Jun 2015 13:29:57

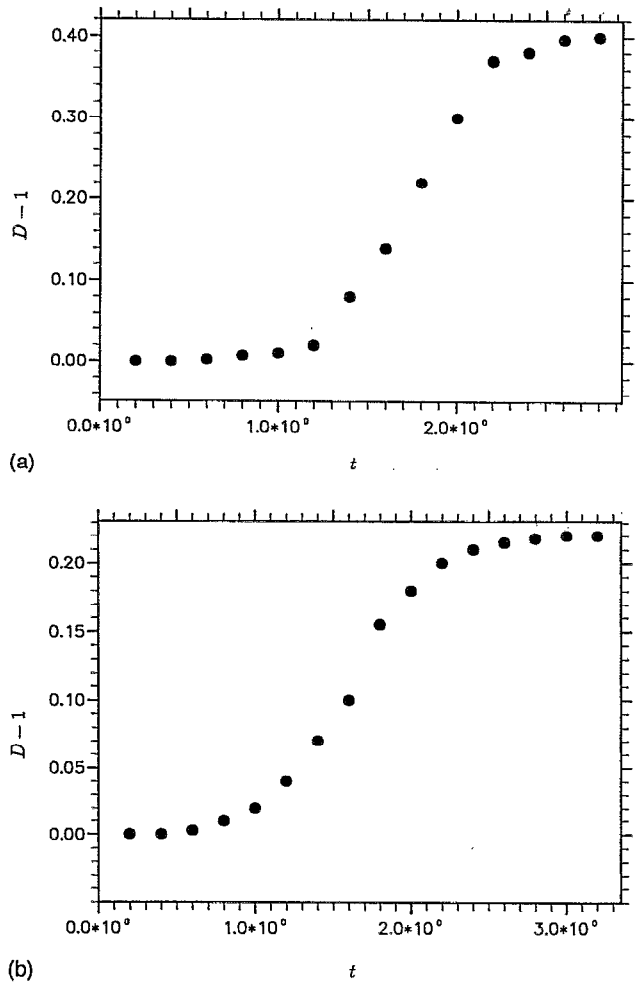

FIG. 9. (a) The dimension D of a line in a SGKS flow reaches a constant value after about 4 Lagrangian time scales. The chosen parameters are the same as in Fig. 8a and D is obtained from the slopes of lines of Figure 8a. (b) The dimension D of a line in a SAKS flow reaches a constant value after about 4 Lagrangian time scales. The chosen parameters are the same as in Fig. 8b and D is obtained from the slopes of the lines of Figure 8b.

turbulent flows. Experimental work on mixing layers has repeatedly shown that mixing is very slow in vortical structures and very rapid in those regions in between where these vortical structures amalgamate (Dimotakis and Brown,[39] Broadwell and Breidenthal[40] and Koochesfahani and Dimotakis[41]). These last regions are in fact convergence regions, and mixing is very fast in them for they stretch interfaces between reactants exponentially fast. In the vortical structures mixing is very slow because interfaces presumably grow only linearly there as they do in our eddy regions. Thus, one may infer from the conclusions summarized in Table IV, that when D_K is dominated by eddy regions and spiral interfacial patterns, D_K distinguishes between those regions of the flow where mixing is fast ($D_K=1$) and those other regions of the flow where mixing is slow ($D_K>1$). However, when D_K is also influenced by tendrils, mixing can also be fast where $D_K>1$.

D. The relation between interfacial capacity and energy spectrum

We release small initially straight lines (smaller than one tenth of the integral length scale) in eddy regions of DKS flows. Such lines become spirals. As the energy spectrum of the turbulence steepens, the capacity D_K of the line decreases (Fig. 19), and is essentially equal to 1 when the spectrum is $E(k)\sim k^{-4}$. Thus, a steepening of the energy spectrum means a 'faster' convergence of the spiral onto its centre. It might also be worth noting that a steeper energy spectrum increases the size of the eddy regions in comparison to the integral scale of the turbulence (Fig. 1).

The result of Fig. 19 is consistent with Redondo's[42] result that the capacity of a density interface in stratified turbulence decreases as the Richardson number increases. Carruthers and Hunt[43] have indeed shown how energy spectra get sharper in stratified turbulence as the Richardson number tends to infinity.

We may also conclude from Fig. 19 and from equation (3.19) in Vassilicos and Hunt[7] that a steepening in the energy spectrum induces a steepening in the scalar power spectrum as well. This is in agreement with Hentschel and Procaccia's result[44] that turbulence intermittency, which entails a steepening of the energy spectrum, also causes the scalar power spectrum's fall off to be sharper.

E. A simple spiral model

We have accounted for the properties of the Kolmogorov capacity of an interface in weakly unsteady 2-D flows ('weakly unsteady' refers to small values of the unsteadiness parameters λ and μ) in terms of eddy regions and spirals. A simple model of the spiraling interfacial mechanism induced by eddy regions can show how D_K may reach an asymptotic steady state where $2>D_K>1$ even though $\overline{|\nabla F|^2}$ increases indefinitely with time and the length of the line increases only linearly with time. Furthermore, in this simple spiral model, D_K is a decreasing function of the power p of the energy spectrum $E(k)\sim k^{-p}$, as is indeed observed in the eddy regions of DKS flows (Fig. 19). In this model, a line winds into a spiral through the action of a point vortex. It is known that the length $l(t)$ of such a spiral grows linearly with time (e.g. see Fung and Vassilicos[10]). Even though the line length in eddy regions of DKS flows increases linearly with time too, eddy regions have in general a more complicated internal structure than a point vortex. Nevertheless, it is interesting to consider one example of a simple flow where D_K is steady, non-trivial and non-space-filling ($1<D_K<2$) and a decreasing function of p, and where $\overline{|\nabla F|^2}\to\infty$ and $L(t)\sim t$ as time t progresses.

As suggested in the beginning of section III, the sustained growth of $\overline{|\nabla F|^2}$ as $t\to\infty$ can be achieved by a gradual increase of the range of scales over which the interface between $F=0$ and $F=1$ is irregular (in case F, as we now assume, is equal to 1 or 0 on either side of the interface) without a need for that interface to become increasingly more space-filling and D_K to reach d (which is $d=2$ here). In other words, for $\overline{|\nabla F|^2}$ to grow with t, it is sufficient that the line interface becomes more space-filling at smaller and

This article is copyrighted as indicated in the article. Reuse of AIP content is subject to the terms at: http://scitation.aip.org/termsconditions. Downloaded to IP: 155.198.172.98 On: Fri, 12 Jun 2015 13:29:57

smaller scales, so that $D_K > 1$ can be measured over smaller and smaller distances without a change of the value of D_K over larger distances. D_K is a significant measure of a persistent feature or constant property of an interface even when the statistics of the interface are changing with time.

For the sake of argument, Fung and Vassilicos[10] assume the point vortex to have an azimuthal velocity $u \sim r^{-q}$ where $q > 0$ and (r, ϕ) are polar coordinates. The energy spectrum

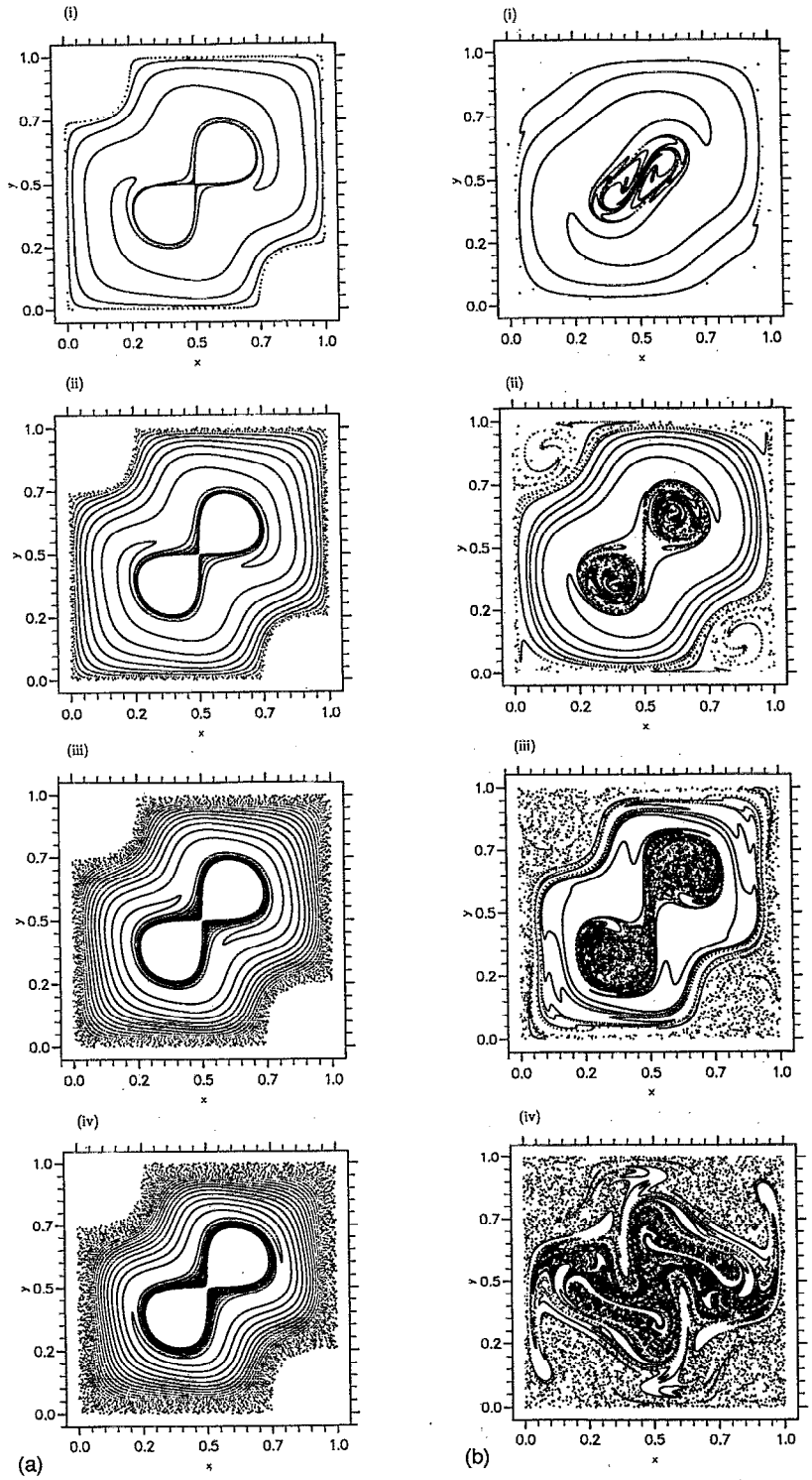

FIG. 10. Examples of spirals and tendrils on a line initially straight, of length 1, with coordinates $y = 0.5$ and x between 0.0 and 1.0 in various SC flows at different time steps (i) $t = 5.0$; (ii) $t = 10.0$; (iii) $t = 20.0$ and (iv) $t = 30.0$. (a) Steady case: with parameters $N_k = 4$, $\mu = 0.0$ and $\lambda = 0.0$ in SC1 flow. (b) Unsteady case: with parameters $N_k = 4$, $\mu = 0.8$ and $\lambda = 0.4$ in SC1 flow. (c) Unsteady case: with parameters $N_k = 4$, $\mu = 0.4$ and $\lambda = 1.5$ in SC1 flow. (d) Unsteady case: with parameters $N_k = 4$ and $\lambda = 0.4$ in SC2 flow.

This article is copyrighted as indicated in the article. Reuse of AIP content is subject to the terms at: http://scitation.aip.org/termsconditions. Downloaded to IP: 155.198.172.98 On: Fri, 12 Jun 2015 13:29:57

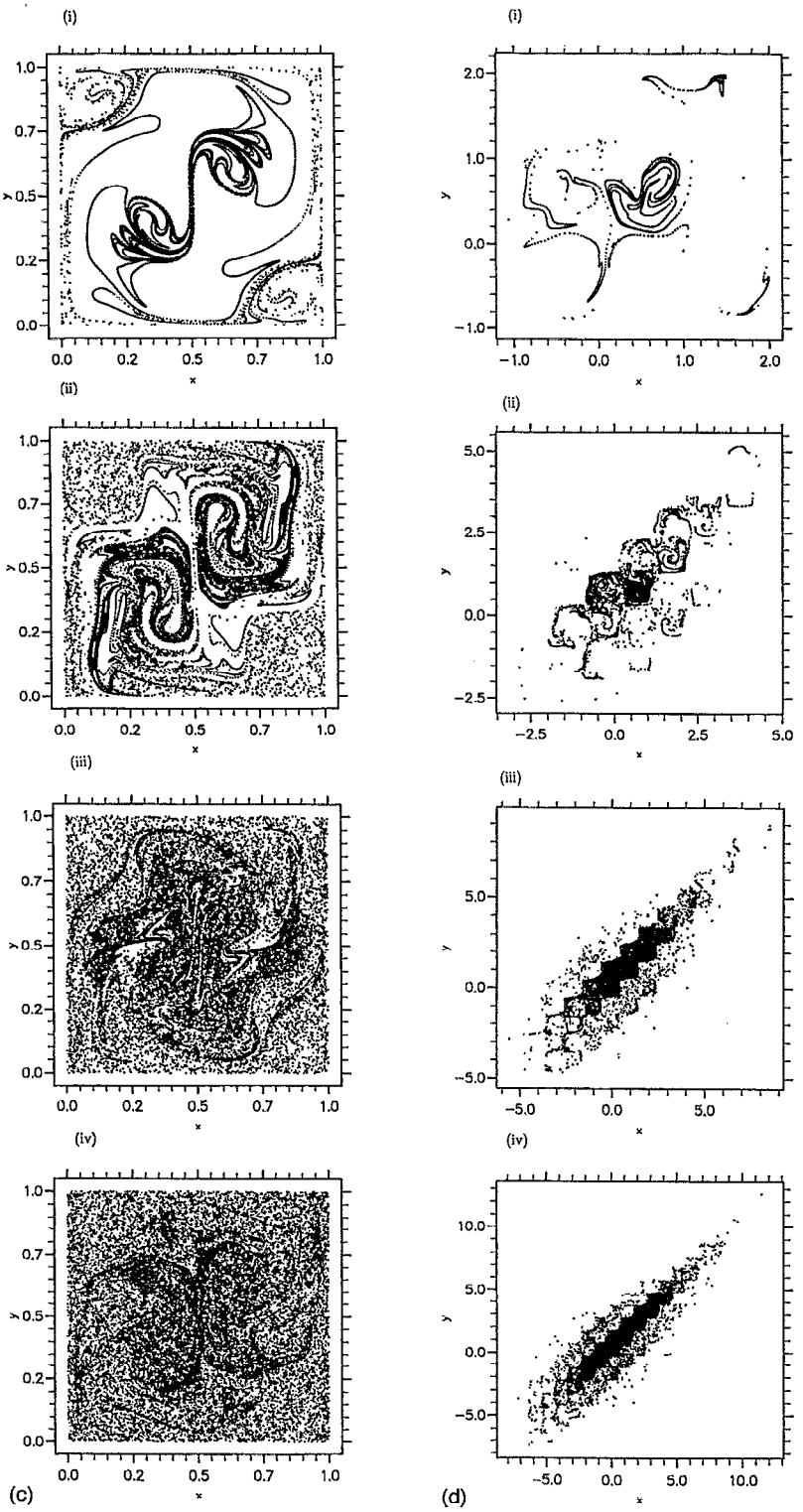

FIG. 10. (*Continued.*)

is defined when $q<1$ and is $E(k)\sim k^{-p}$ where $p=3-2q$. When $q=1$, this velocity field is the well known point vortex solution of the Euler equation. A line released within the vortex adopts, at time t, the spiral form

$$r(\phi)\sim\left(\frac{\phi}{t}\right)^{-1/(1+q)}. \tag{42}$$

The Kolmogorov capacity D_K of the spiral depends only on the power $1/(1+q)$ and is smaller than $d=2$ for all finite values of q (see Vassilicos and Hunt[6]). D_K is therefore independent of time and non-trivial.

It is simpler (see Vassilicos and Hunt[6]) to work with the Kolmogorov capacity D'_K of the intersections of the spiral

This article is copyrighted as indicated in the article. Reuse of AIP content is subject to the terms at: http://scitation.aip.org/termsconditions. Downloaded to IP: 155.198.172.98 On: Fri, 12 Jun 2015 13:29:57

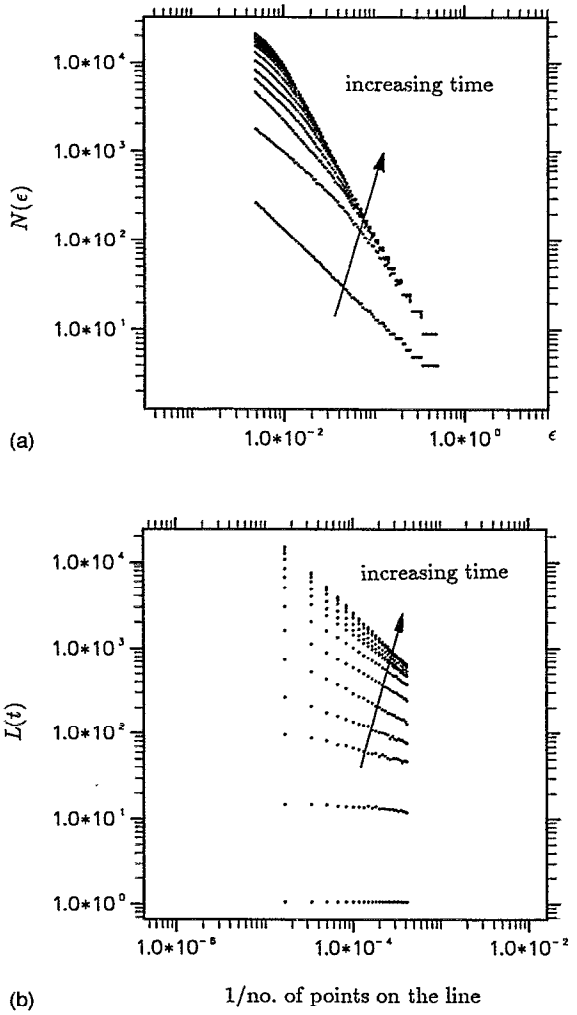

FIG. 11. (a) Example of a log–log plot of $N(\epsilon)$ vs. ϵ for different times in the evolution of a line in a SC1 flow (the parameters are $N_k=4$, $\mu=0.6$ and $\lambda=1.0$). The slope of the power law increases with time and reaches a constant value after $t=10$ ($T_L\approx 1.4$). Such well defined asymptotic power laws are also observed in SC2 flows. (b) Example of a log–log plot of $L(t)$ versus resolution (1/No. of points on the line) for different times in the evolution of a line in a SC1 flow. The parameters are those of Fig. 11a. Note that the slope of the power law increases with time and reaches a constant asymptotic value after $t=22$ ($T_L\approx 1.4$). Such well defined asymptotic power laws are also observed in SC2 flows.

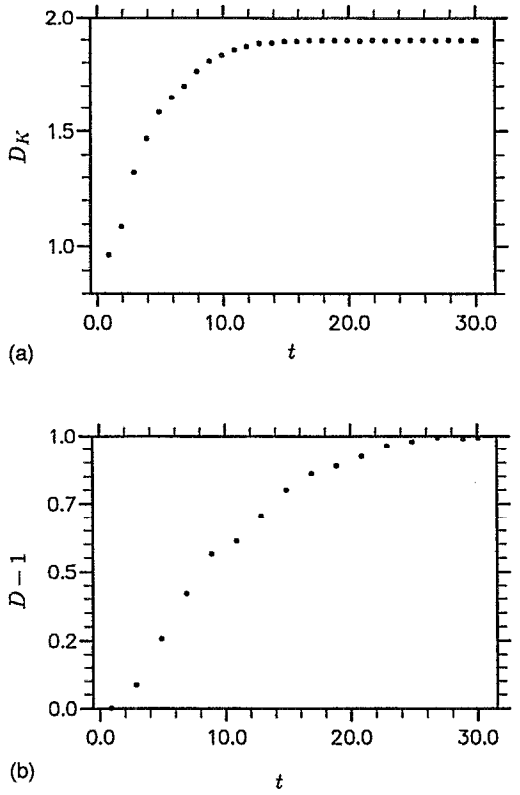

FIG. 12. (a) Example of an SC1 flow where the capacity D_K reaches an asymptotic constant value of 1.9. The chosen parameters are those of Fig. 11a and D_K is obtained from the slopes of the lines of Figure 11a. The Kolmogorov capacity D_K is also observed to asymptote to a constant value in SC2 flows but not as quickly as in the KS flows ($T_L\approx 1.4$ in the SC flows). (b) Example of an SC1 flow where the dimension D reaches an asymptotic constant value of 1.0. The chosen parameters are those of Fig. 11b and D is obtained from the slopes of the lines in Figure 11b. The dimension D is also observed to asymptote to a constant value in SC2 flows but not as quickly as in the KS flows ($T_L\approx 1.4$ in the SC flows).

with a straight line; $0\leqslant D'_K\leqslant 1$. The Kolmogorov capacity D_K of the spiral is an increasing function of D'_K, and

$$D'_K=\frac{1}{1+\dfrac{1}{1+q}}=\frac{q+1}{q+2}=\frac{5-p}{7-p} \tag{43}$$

(see Vassilicos and Hunt[6]). D'_K is a decreasing function of p, and therefore so is D_K.

It is also easier in this context to deal with the average over space of $|\nabla F|$ than with $\overline{|\nabla F|^2}$. If A is the area of a finite portion of 2-D space where the entire spiral lies, then (see Vassilicos and Hunt[45])

$$\frac{1}{A}\int_A |\nabla F|\, dS=\frac{l(t)}{A}\sim t, \tag{44}$$

since $l(t)\sim t$ for all values of $q>0$ (see Fung and Vassilicos[10]).

The spirals obtained in our 2-D DKS, SAKS and SGKS flows are clearly (by direct inspection of Fig. 4) more complex than those obtained through the action of a point vortex. This model shows clearly though how a spiraling line can have a capacity that is non-trivial and constant in time, and yet a length $l(t)\sim t$ and a $\overline{|\nabla F|}$ that grows with time indefinitely. The model also predicts that D_K should decrease as the energy spectrum steepens.

Furthermore, numerical experiments with a line interface in a single oscillating point vortex show that the Kolmogorov capacity D_K of the interface decreases as the frequency ω of the oscillation increases, at least for small enough values of ω. The centre of the point vortex is made to oscillate along the x-axis according to $x_0=\xi\sin(\omega t)$, where x_0 is the x-coordinate of the centre of the vortex, and ξ the spatial

This article is copyrighted as indicated in the article. Reuse of AIP content is subject to the terms at: http://scitation.aip.org/termsconditions. Downloaded to IP: 155.198.172.98 On: Fri, 12 Jun 2015 13:29:57

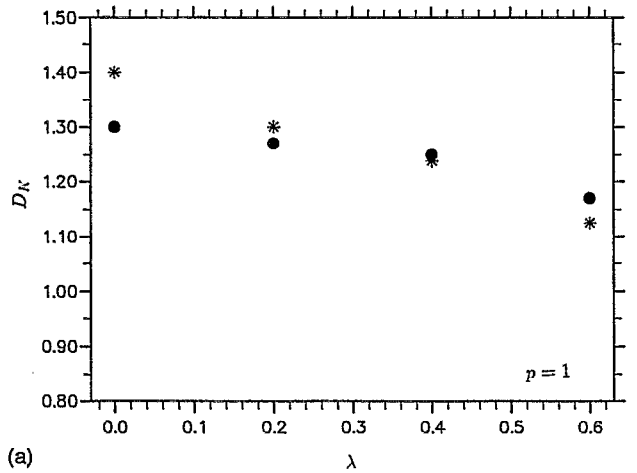

(a)

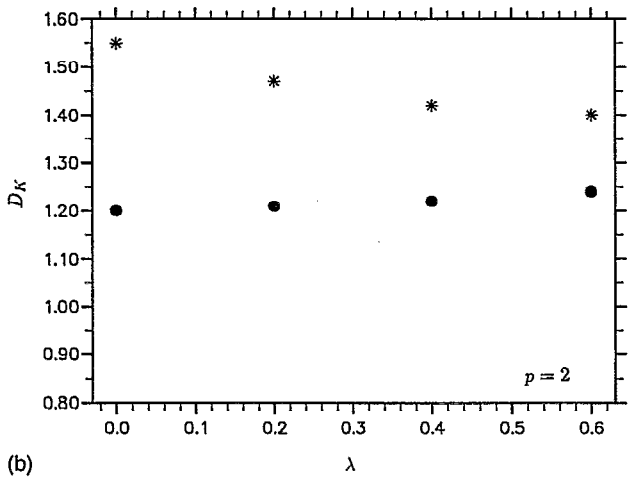

(b)

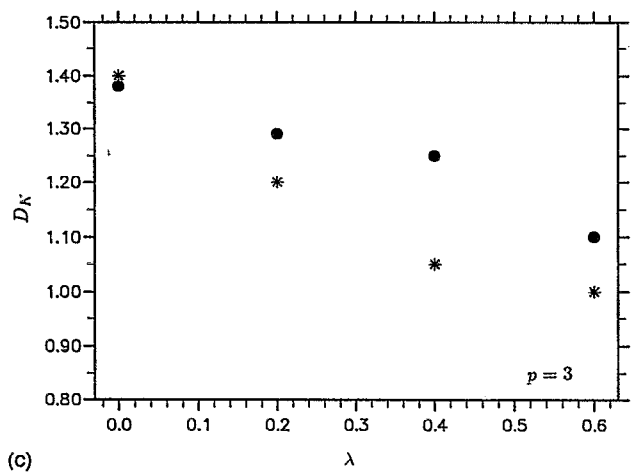

(c)

FIG. 13. The capacity D_K is a decreasing function of unsteadiness in the SAKS flows that we tested, except in the case where $p=2$. The symbols **** for SGKS; ●●●● for SAKS. (a) $p=1$; (b) $p=2$; (c) $p=3$.

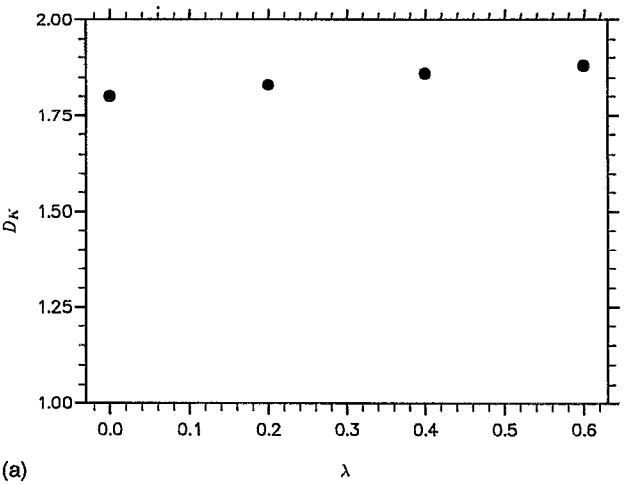

(a)

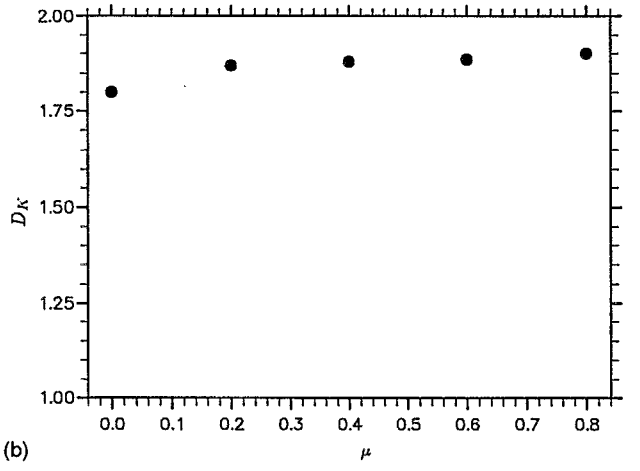

(b)

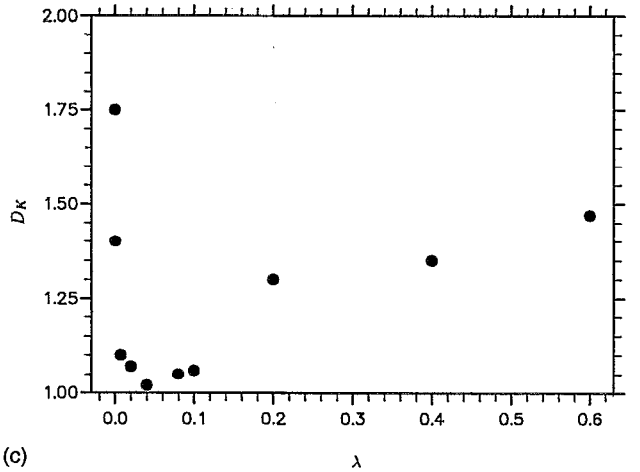

(c)

FIG. 14. (a) D_K is a slowly increasing function of λ in a SC1 flow where $\mu=0.8$. (b) D_K is a slowly increasing function of μ in a SC1 flow where $\lambda=1.0$. (c) D_K first decreases with increasing λ for very small values of λ, then increases with increasing unsteadiness for larger values of λ in a SC2 flow.

amplitude of the oscillation. The radial velocity induced by the vortex (radial towards the instantaneous centre of the vortex) is identically zero, and the azimuthal velocity (relative to the instantaneous centre) is $u_\phi=\Gamma/(2\pi r)$ (i.e. $q=1$), where Γ is the total circulation and r the radial distance to the vortex centre. We limit our experiments to the case where the only dimensionless parameter of the problem, $\xi^2\omega/\Gamma$, is much smaller than 1. Specifically, in the present runs, $0\leqslant\xi^2\omega/\Gamma\leqslant 0.04$. Fig. 20a shows the spiral generated from the wrapping of a line around the point vortex when $\omega=0$,

This article is copyrighted as indicated in the article. Reuse of AIP content is subject to the terms at: http://scitation.aip.org/termsconditions. Downloaded to IP: 155.198.172.98 On: Fri, 12 Jun 2015 13:29:57

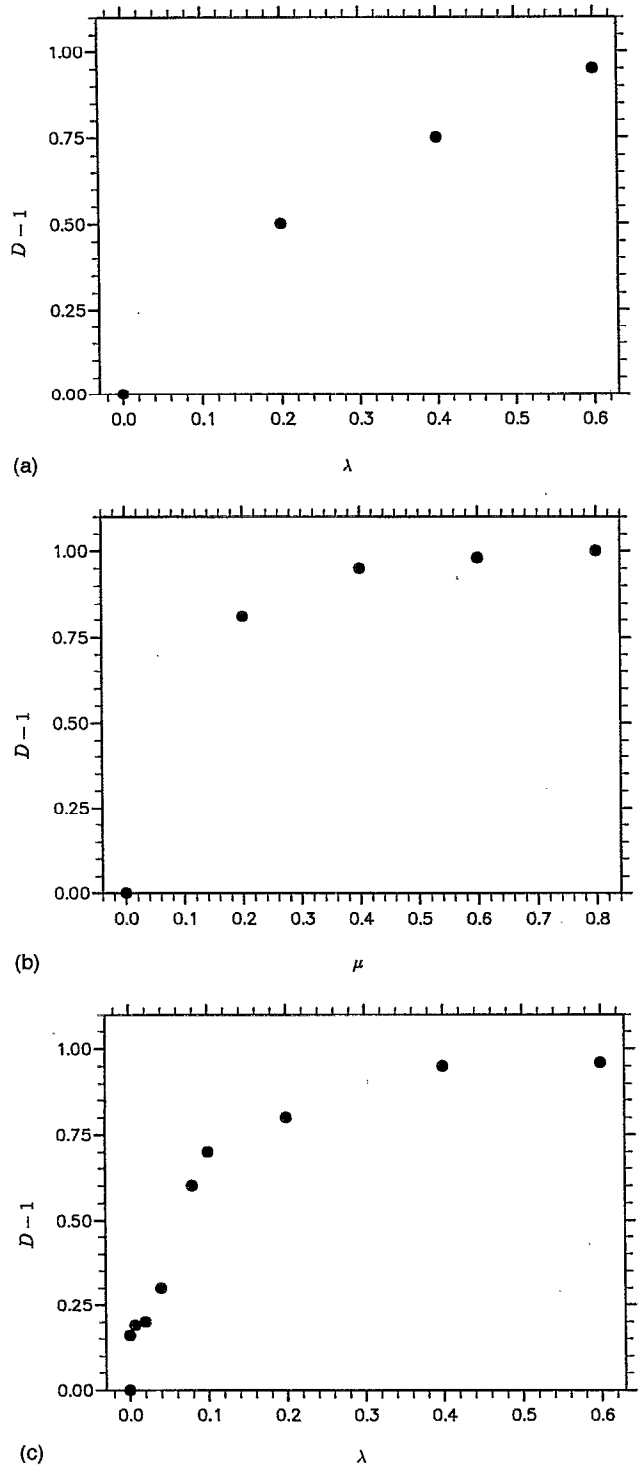

FIG. 15. (a) D is an increasing function of λ in a SC1 flow where $\mu=0.8$. (b) D is an increasing function of μ in a SC1 flow where $\lambda=1.0$. (c) The dimension D is an increasing function of λ in a SC2 flow.

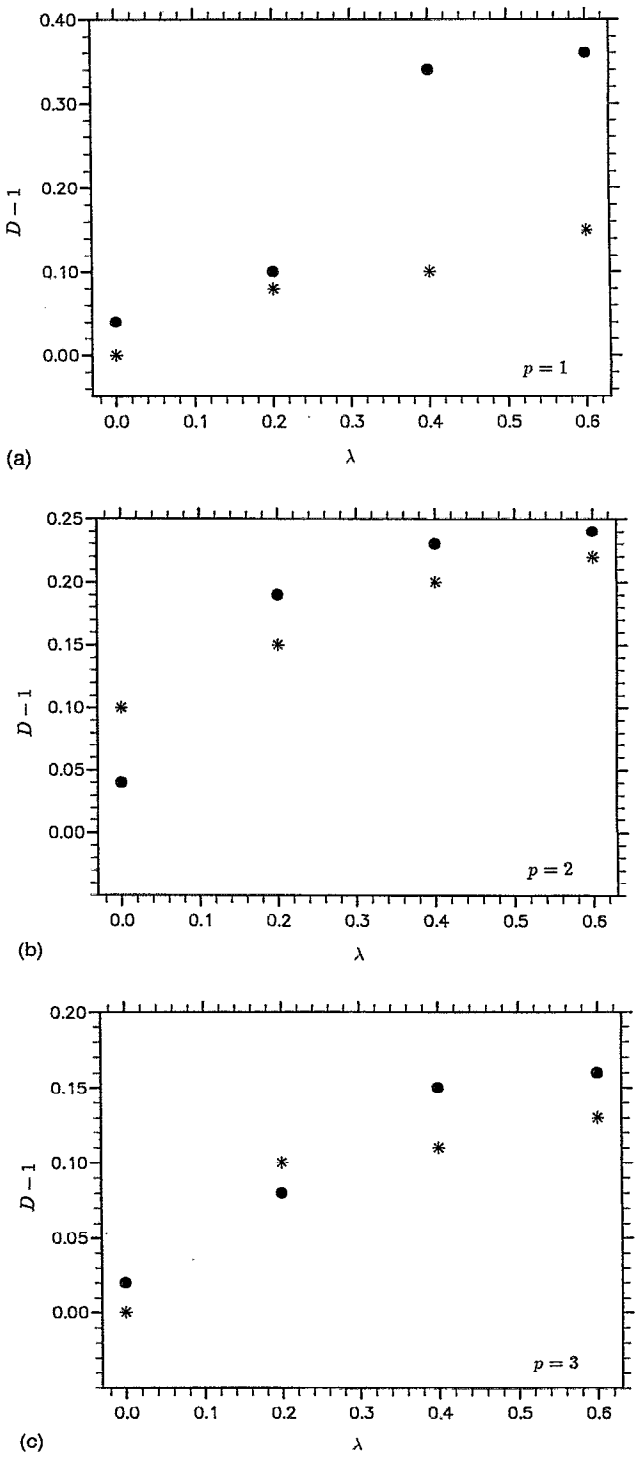

FIG. 16. The dimension D is an increasing function of the unsteadiness parameter λ both in SGKS **** and SAKS ●●●● with different values of p. (a) $p=1$; (b) $p=2$; (c) $p=3$.

and Fig. 20b is a plot of the line interface at the same time in an oscillating point vortex with $\xi^2\omega/\Gamma=1.2\times10^{-3}$. From (43), $D'_K=2/3$ for a non-oscillating point vortex with $q=1$, and from Vassilicos and Hunt,[6] $D_K=2D'_K=1.33$. Fig. 21 shows that the Kolmogorov capacity D_K of a line in an oscillating point vortex decreases below 1.33 as the frequency ω increases, at least in the range where $\xi^2\omega/\Gamma\ll1$. For such small values of the dimensionless parameter $\xi^2\omega/\Gamma$, insofar as the Kolmogorov capacity D_K is concerned, the topology of the interface is spiral. Hence, as long as the topology of the interface is essentially spiral, we may expect the Kolmogorov capacity of a line to be a decreasing function of

This article is copyrighted as indicated in the article. Reuse of AIP content is subject to the terms at: http://scitation.aip.org/termsconditions. Downloaded to IP: 155.198.172.98 On: Fri, 12 Jun 2015 13:29:57

TABLE II. General rule for D in SC1, SC2, SAKS and SGKS flows.

2-D flow	Steady	Unsteady, $N_k=4$	Unsteady, $N_k=60$, 100
Dimension D	$D=1$	$0<D-1\leqslant 1$	$0<D-1\ll 1$

unsteadiness, as we indeed observe in some of our KS and SC flows.

F. Does the distribution of wavenumbers affect the properties of the interface? A third mechanism for generating complex interfacial topology

The wavemodes that dominate two-particle dispersion are the ones at the high wavenumber end of the energy spectrum (Batchelor[46]). We therefore expect the small-scale topology of the interface to be determined by the high wavenumber end of the energy spectrum too. But does the *distribution* of the large wavenumbers affect the scaling properties of the interface's topology?

In Fig. 2 we plot $\Delta k_n k_n^2 U^2[k_n$ for two different distributions of wavenumbers k_n, one algebraic (SAKS flows) the other geometric (SGKS flows)]. In both cases $U(k_n)$ is drawn at random from a probability distribution of mean zero and variance given by (19). It is clear from Fig. 2 that the difference between the two distributions of wavemode energies is small for identical energy spectra $E(k)$, particularly at the high wavenumbers ($k>20$), where it is practically imperceptible. It has been recently suggested that flows such as SAKS and SGKS may be used to simulate deep ocean and coastal small-scale dispersion realisation by realisation (Perkins *et al.*,[47] Perkins and Fung[48]). The rate of dispersion, and in particular, burning and chemical reaction rates across dispersing interfaces depend crucially on the topology and the scaling exponents (such a D_K) of these interfaces. Can the imperceptible difference in the high wavenumber Fourier distribution of energy that distinguishes SAKS from SGKS flows have significant consequences on the topology and/or the scaling of a passively advected interface at scales below $2\pi/k_{N_k}$?

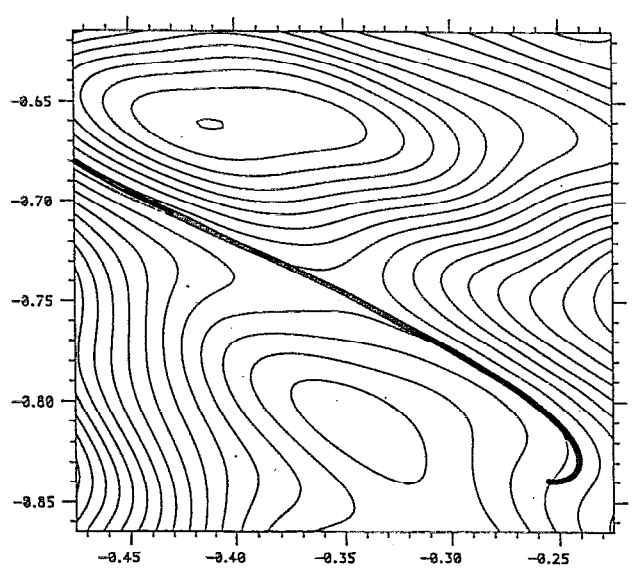

FIG. 17. Line initially in a convergence region with a streamlined background. The initial length is $1/12(=L_T/12)$, and $t=0.3T_L$.

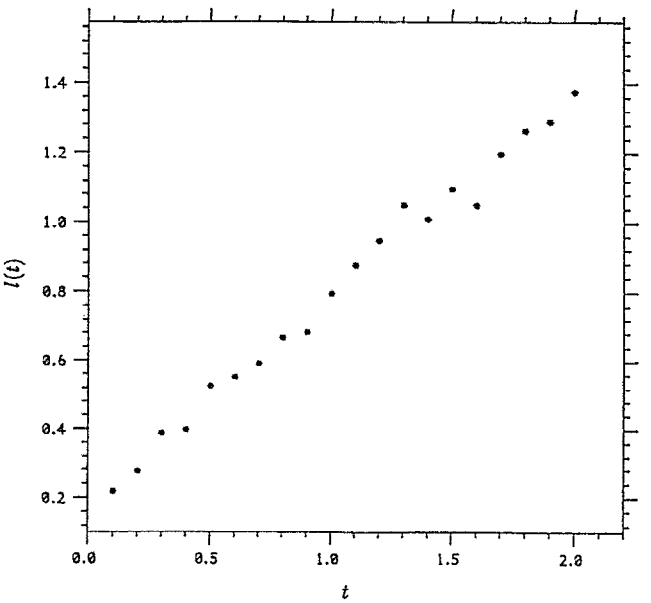

FIG. 18. The growth of the length of a line in an eddy region. The unit of time is $T_L\approx 1$.

We measure the D_K of the interface over two decades of scales below $2\pi/k_{N_k}$, i.e. the size ϵ of the boxes in the box-counting algorithm is such that $(2\pi/k_{N_k})\times 10^{-2} \leqslant \epsilon \leqslant 2\pi/k_{N_k}$. We do so for interfaces in single realisations of SAKS and SGKS flows for various values of p and λ, and we also measure D. The line-interfaces are initially very long and are therefore spanning a large variety of flow regions (L_0 is equal to one integral length scale of the flow). The results are plotted in Figs. 13 and 16. In most unsteady cases, D is larger in the SAKS rather than in the SGKS flows, and always increases with λ. In particular, when $p=1$ the difference between the values of D in unsteady SAKS and SGKS flows is substantial. However, when $p=1$ the difference between the values of D_K in SAKS and SGKS flows is insignificant, but is more significant when $p=3$, and D_K decreases with λ in both SAKS and SGKS flows when $p=1$ and $p=3$. The case where $p=2$ is the most striking. Whilst D_K decreases with increasing λ in SGKS flows, it does not decrease with λ in SAKS flows. Furthermore, the difference between the values of D_K in either flows is maximal, and in fact very large when the flows are steady.

These results are evidence of a complex interaction between the effects of unsteadiness and those of the distribution of wavenumbers. Different distributions of wavenumbers can produce different interfacial scaling properties even when the energy spectrum of the flow is kept constant. The difference between algebraic and geometric distributions of wavenumbers is imperceptible at high wavenumbers, but it

This article is copyrighted as indicated in the article. Reuse of AIP content is subject to the terms at: http://scitation.aip.org/termsconditions. Downloaded to IP: 155.198.172.98 On: Fri, 12 Jun 2015 13:29:57

TABLE III. General rule for D_K and local line growth in DKS flows.

	Eddy regions	Convergence regions
Capacity D_K	$D_K>1$	$D_K=1$
Line Growth	Slow ($l(t) \propto t$)	Fast ($l(t) \propto e^{at}$)

can cause dramatic differences in the scaling exponents of the interface and their dependence on the degree of unsteadiness. As we mentioned in section II.C the distribution of wavenumbers can determine whether the velocity field is H-fractal or K-fractal.

Berry *et al.*[8] identified two mechanisms for generating complex interfacial topology, both based on the topology of path-lines around elliptic (eddy regions) and hyperbolic (convergence regions) points. We are now confronted with a third mechanism, which relates to the velocity profile *across* streamlines. In streaming regions, for example, where the curvature of streamlines is small (see Fig. 1), we can think of the velocity profile as one-dimensional and given by (22) where x is a coordinate normal to the streamlines and $u(x)$ is the velocity along the streamlines. If the flow is steady, a line-interface initially straight and along the x-axis will develop a shape that is a direct imprint of the velocity profile across streamlines. If that profile is H-fractal (K-fractal), the line will become H-fractal (K-fractal) too. We mentioned in section II.C that for identical energy spectra, $u(x)$ may be either H- or K-fractal depending on the distribution of wavelengths λ_n in (22). The length of the line at a time $t\to\infty$ is $L(t)\approx t\int_0^{L_0}|du/dx|dx$; in practise the line has only finite resolution and is represented by N_0 points where $N_0=L_0/\epsilon_0$. The measured value of the line length is

$$L(\epsilon_0,t)\approx t\epsilon_0\sum_{i=1}^{N_0-1}\left|\frac{\Delta u_i}{\epsilon_0}\right|, \tag{45}$$

where Δu_i is the difference of velocities between points i and $i+1$ on the line originally ($t=0$) at a distance ϵ_0 from each other. If the distribution of wavelengths is such that $a_n/\lambda_n\to 0$ as $n\to\infty$ at a rate that is fast enough for $\Sigma_{n=1}^{+\infty}a_n/\lambda_n$ to be finite, then the velocity profile is nearly everywhere smooth and not H-fractal (see section II.C) and $|du/dx|$ is also finite and bounded from above by $2\pi\Sigma_{n=1}^{+\infty}a_n/\lambda_n$. Thus, $L(\epsilon_0,t)<t\epsilon_0 N_0 2\pi\Sigma_{n=1}^{+\infty}a_n/\lambda_n = tL_0 2\pi\Sigma_{n=1}^{+\infty}a_n/\lambda_n$, which implies that $D=1$ in agreement with the fact that the line is not H-fractal since it takes the shape of the velocity profile.

On the other hand, when $a_n/\lambda_n\to\infty$ as $n\to\infty$, du/dx does not exist and the velocity profile is H-fractal; however, $\Delta u_i/\epsilon_0$ is finite but tends to infinity as $\epsilon_0\to 0$ at nearly all points i. Hence, $\Sigma_{i=1}^{N_0-1}|\Delta u_i/\epsilon_0|$ tends to infinity at a rate faster than $N_0=L_0/\epsilon_0$, so that if D is well defined it must be greater than 1 ($D>1$). This agrees with the fact that the line adopts the H-fractal shape of the velocity profile.

TABLE IV. General rule subject to exceptions as explained in the text.

Dominant interfacial feature	Spirals	Tendrils
Capacity D_K	Decreasing with unsteadiness	Increasing with unsteadiness
Dimension D	$0<D-1<<1$	$0<D-1\leqslant 1$

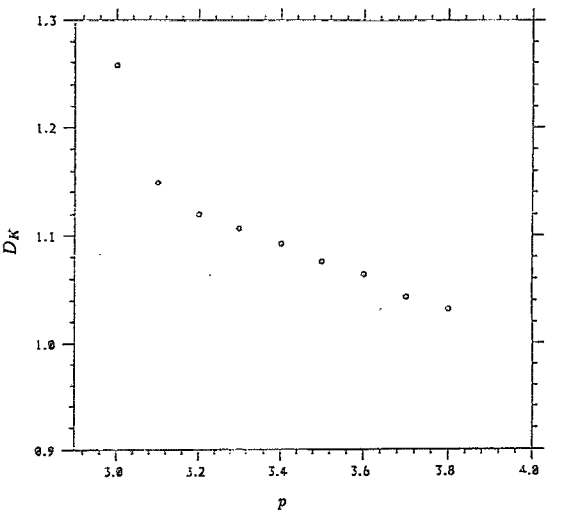

FIG. 19. Relation between the Kolmogorov capacity D_K and the energy spectrum's fall off, i.e. the exponent p in $E(k)\sim k^{-p}$. The values of D_K are taken at time $t=2.0T_L$ from a line in a DKS flow.

The above discussion demonstrates how different wavenumber distributions can generate different scaling topologies and different values of D even when the energy spectrum is kept constant. Our numerical simulations indicate that a change in the distribution of wavenumbers can also change the value of D_K and the dependence of D_K on the unsteadiness parameter λ.

IV. CONCLUSION

Interfaces occur in many turbulent reacting flows, e.g. between chemically different fluids or between burnt and unburned fuel. In such cases, it is the area per unit volume of the interface (or the length per unit area of the line-interface in 2-D flows) that essentially determines chemical reaction rates and turbulent flame speeds (combustion rates). In turn, this area per unit volume may be a simple function of the fractal dimension and of the smallest length scale of the interface. Problems involving flow dispersion and chemical reaction may be considered solved once the fractal dimension and the range over which that dimension is defined are known.

However, turbulent flows are not the only flows that produce fast mixing. Chaotic advection also generates very complex interfacial topologies. Furthermore, turbulence may not have a universal structure, so that different turbulent flows may generate different interfacial geometries (see Hunt *et al.*[49]). Given a flow, do fractal dimensions exist? If they exist, is their value non-trivial and do they asymptote to a steady value in time regardless of the incessant deformation (stretching and bending) of the interface by the flow? And finally, how can these fractal dimensions be calculated from the properties and parameters of the flow? Conversely, it may

This article is copyrighted as indicated in the article. Reuse of AIP content is subject to the terms at: http://scitation.aip.org/termsconditions. Downloaded to IP: 155.198.172.98 On: Fri, 12 Jun 2015 13:29:57

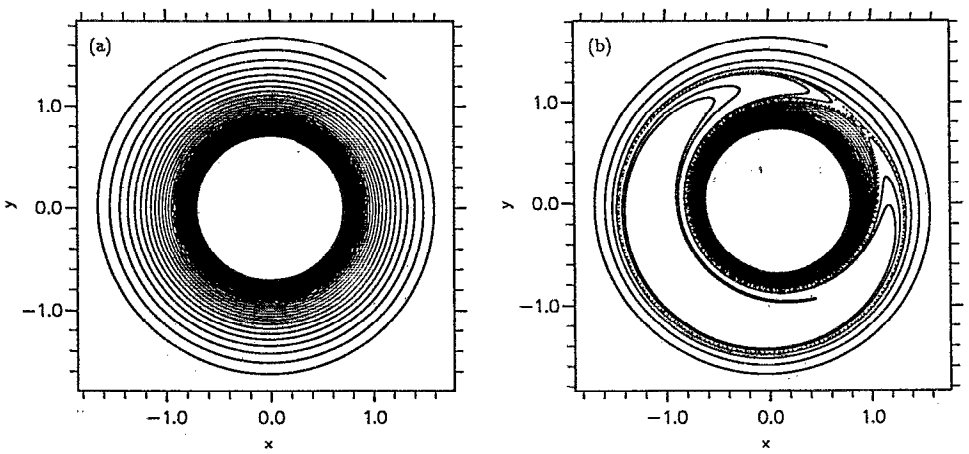

FIG. 20. Line interface at time $t=300$ in a point vortex of circulation $\Gamma=2.5$; (a) the vortex is not oscillating ($\omega=0$); (b) the vortex is oscillating with frequency $\omega=0.3$ and spatial amplitude $\xi=0.1$.

be interesting to know what can be deduced about a flow from measurements of interfacial fractal dimensions. The topology, the scalings and the degree of space-fillingness of an interface could serve as a probe into the space, the time and the wavenumber-space structures of the flow. This paper is a contribution towards a theory that can answer the above questions.

Our first result is that the Kolmogorov capacity D_K and the dimension D of line-interfaces in 2-D turbulent-like flows are well-defined and tend to constant steady state values in finite time. That finite time is $O(T_L)$ in those flows where the number of degrees of freedom N_k is $O(10^2)$, and $O(10T_L)$ in the SC flows where $N_k=O(1)$. Even though the flow continues to act on the interface over times longer than T_L, D_K is always *strictly* in between the trivial value 1 and the space-filling value 2. $D-1=0$ when the flow is steady and $D-1>0$ when the flow in unsteady. However, in unsteady flows, $D-1$ is small ($D-1\ll 1$) when the number of degrees of freedom (wavenumbers) N_k of the flow is large ($N_k=100$) and $D-1$ is large ($D-1\leqslant 1$) when N_k is small ($N_k=4$). The interface is H-fractal only when $D>1$. The dimension D may be interpreted to be a *degree* of H-fractality, which, in unsteady 2-D flows, is found to be small when N_k is large and large when N_k is small.

The concept of a 'degree of H-fractality' can be thought of from a different (and complementary) perspective if we recall Berry *et al.*'s[8] remark that the topology of the interface is affected by the elliptic points of the flow which generate isolated spirals on the interface, and by the hyperbolic points of the flow near where the interface acquires a tendril-like topology and is H-fractal. Other flow regions, such as the streaming regions (Wray and Hunt[7]), do not influence the topology of the interface significantly unless the structure of the flow in *wavenumber-space* is such that the velocity profile across streamlines is itself topologically non-trivial. As indicated by the study of Weierstrass functions, very subtle differences in the *distribution* of wavenumbers can cause dramatic qualitative differences in the velocity profile's topology even when the energy spectrum and the phases are kept constant. We observe in numerical experiments that a change of wavenumber distribution from geometric to algebraic changes the values of the Kolmogorov capacity D_K and the dimension D of the interface, and can even change the character of D_K's dependence on the unsteadiness parameter of the flow from decreasing to slowly increasing.

When the flow is steady and $D-1=0$, there is no H-fractality whatsoever, and the value of D_K is dominated by the spiral topology of the interface around elliptic points. When the flow is unsteady and the number of degrees of freedom N_k is small, $D-1$ is small when the topology of the line appears to be dominated by isolated spirals (which does not mean that tendrils do not exist but that they are less conspicuous than the isolated spirals); $D-1$ is large (closer to 1) when the line is dominated by the H-fractal structure of chaotic tendrils. We find that $D-1$ always increases with unsteadiness; unsteadiness is a chaos generating mechanism (as shown by Aref[29]—see also Ottino[9]) and an increase in unsteadiness increases the degree of H-fractality of the inter-

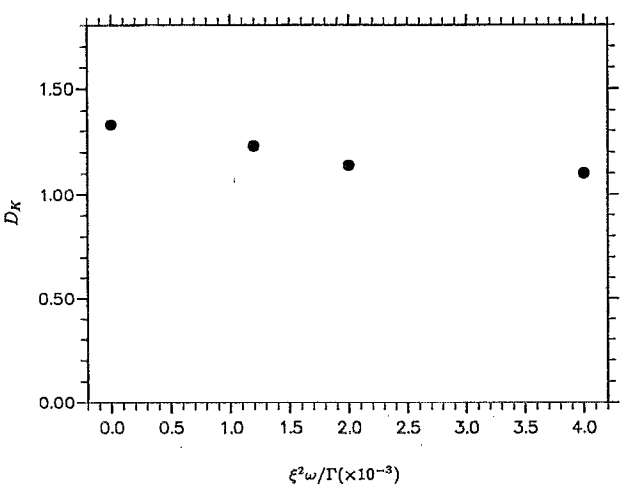

FIG. 21. The Kolmogorov capacity D_K of a line interface in an oscillating point vortex as a function of $\xi^2\omega/\Gamma$. Note that $D_K=1.33$ when $\omega=0$, and decreases with increasing ω.

This article is copyrighted as indicated in the article. Reuse of AIP content is subject to the terms at: http://scitation.aip.org/termsconditions. Downloaded to IP: 155.198.172.98 On: Fri, 12 Jun 2015 13:29:57

face by increasing the chaotic tendril structures at the expense of the spiral structures.

Our results indicate that a relation exists between the type of interfacial topology (whether spirals or tendrils) and the dependence of D_K on the unsteadiness. As a general rule, D_K decreases with increasing unsteadiness when the topology is dominated by spirals, and the degree of H-fractality is small; D_K increases with unsteadiness when the topology is dominated by chaotic tendrils, and the degree of H-fractality is high. A flow with small N_k and *confined* within a region surrounded by fluid paths that coincide with streamlines generates interfaces with a topology that is dominated by chaotic tendrils and D_K increases with unsteadiness. In unconfined flows with a small number of degrees of freedom, D_K first decreases and then increases beyond a threshold unsteadiness where the topology changes from being dominated by spirals to being dominated by chaotic tendrils. When the number of degrees of freedom is large ($N_k=100$), in most cases we observe a decrease of D_K with increasing unsteadiness, and $D-1$ is never large. However, it is hard to judge from the pictures of interfaces which of the spiral or the tendril structures dominate the scaling of the topology. Perhaps surprisingly, the dependence of D_K on the unsteadiness can be transformed from decreasing to non-decreasing by changing the distribution of modes in wavenumber space without changing the phases and the energy spectrum. The distribution of wavenumbers can significantly affect the values of D_K and D. We argue that the distribution of wavenumbers can have a decisive qualitative effect on the scalings and the topology of the interface. Thus, along with hyperbolic and elliptic points, the distribution of modes in Fourier space is another important factor in the development of interfacial scalings and topology when N_k is large.

We obtain further insight and corroborate the interpretation of our previous results from the study of a line winding inside a simple vortex. When the vortex is steady, we can show analytically that D_K is constant in time and that $1<D_K<2$ even though the length $L(t)$ of the line increases indefinitely and not exponentially ($L(t)\sim t$). Furthermore, we show analytically that D_K is a decreasing function of the exponent p of the self-similar energy spectrum ($E(k)\sim k^{-p}$) of the vortex, a property which we also observe in the eddy regions of our 2-D turbulent-like flows. Numerical experiments carried out with a point vortex oscillating in space corroborate that D_K decreases with increasing unsteadiness when the flow-generated interfacial topology is essentially spiral.

ACKNOWLEDGEMENTS

We are grateful to J.C.R. Hunt for valuable discussions. JCHF and JCV acknowledge financial support from the University of Hong Kong Science and Technology under Grant No. DAG92/93.SC13 and JCV acknowlegdes financial support from the European Community under Contract No. CHRX-CT92-00091.

APPENDIX: THE DIMENSION D AND THE HAUSDORFF DIMENSION D_H OF AN EVOLVING INTERFACE

To prove that $D>1$ is a sufficient and necessary condition for a line that evolves in a flow field to be H-fractal, we must prove that the line's Hausdorff dimension D_H is strictly larger than 1 when and only when $D>1$. Provided D exists and is well-defined, it is equivalent to show that $D_H=1$ if and only if $D=1$, because both D_H and D can never be smaller than 1. Here we show that $D=1$ implies $D_H=1$; and that $D_H=1$ implies $D=1$ if we assume that the velocity field has no finite time singularities over vanishingly small scales.

The dimension D was introduced by Fung and Vassilicos[10] and is defined in (41). To define the Hausdorff dimension D_H of a line we must first define the Hausdorff measure $H_\Delta(\epsilon)$. Consider a covering of the line with disks of variable sizes ϵ_i. The Hausdorff measure $H_\Delta(\epsilon)$ is, by definition,

$$H_\Delta(\epsilon)=\inf\sum_i \epsilon_i^\Delta, \tag{A1}$$

where the infimum extends to all possible countable coverings subject to the constraint $\epsilon_i\leqslant\epsilon$. Hausdorff proved (see Falconer[17]) that as $\epsilon\to 0$, $H_\Delta(\epsilon)$ tends to either ∞ or 0 according to whether Δ is strictly smaller or strictly larger than a critical number D_H. That critical number is the Hausdorff dimension, and at that critical value $\Delta=D_H$, the Hausdorff measure may tend to either a finite or a non-finite value as $\epsilon\to 0$. A line is H-fractal if and only if $D_H>1$, and an example of an H-fractal is the Koch curve or a line-interface in a blinking vortex (see Fung and Vassilicos[10] for pictures of these H-fractal curves). When $D_H=1$, the line is either everywhere smooth, or has at most a *countable* number of *isolated* singularities such as spirals.

We use N points to resolve the evolving line, and δ_i ($i=1,2,\ldots,N$) are the distances between consecutive simulated points i and $i+1$ on the line at time t ($\delta_i=\delta_i(t)$). When either $D=1$ or $D_H=1$, a complete covering of the line including both simulated and unsimulated points is possible at time t with disks of sizes $\epsilon_i=\delta_i$ for times t that are small enough, say smaller than τ. The time τ depends on the initial resolution of the line, i.e. $\tau=\tau(\epsilon_0)$ where $\epsilon_0=L_0/N_0$, L_0 is the initial length of the line and N_0 the number of points constituting the numerical resolution of the line. Thus, for $t<\tau(\epsilon_0)$,

$$H_\Delta(\epsilon,t)\leqslant\sum_i \delta_i^\Delta; \tag{A2}$$

where $\epsilon=\sup_i\delta_i$. The length scale ϵ is a function of both ϵ_0 and time t, i.e. $\epsilon=\epsilon(\epsilon_0,t)$, and tends to 0 as $\epsilon_0\to 0$.

Let us first show that $D=1$ implies $D_H=1$. A special case of equation (A2) is obtained when $\Delta=1$:

$$H_1(\epsilon,t)\leqslant\sum_i \delta_i=L(\epsilon_0,t). \tag{A3}$$

If $D=1$, then $L(\epsilon_0,t)$ remains finite as $\epsilon_0\to 0$—see (41)—, and as a consequence, $H_1(\epsilon)$ also remains finite as $\epsilon\to 0$.

This article is copyrighted as indicated in the article. Reuse of AIP content is subject to the terms at: http://scitation.aip.org/termsconditions. Downloaded to IP: 155.198.172.98 On: Fri, 12 Jun 2015 13:29:57

Hence, $D_H=1$. We have therefore shown that $D=1$ implies $D_H=1$ which is equivalent to the statement that $D_H>1$ implies $D>1$.

Let us now show the converse, i.e. that $D_H=1$ implies $D=1$. When $D_H=1$, the line is either everywhere smooth at any finite time t, or has at most a *countable* number of *isolated* singularities *over vanishingly small scales* at a *finite* time t (see Vassilicos and Hunt[6]). Such singularities may occur only if the line crosses a point where the flow velocity is infinite (such as the centre of a point vortex), or undefined because of accumulating velocity fluctuations over vanishingly small scales at that point. Our assumption that finite time flow singularities do not exist means that the velocity field is everywhere neither infinite nor undefined at all finite times. The line is therefore everywhere smooth at all finite times, and $H_1(\epsilon,t)$ remains finite as $\epsilon\to 0$. Because $H_1(\epsilon,t)$ approximates the length of the line,

$$L(\epsilon_0,t)-H_1(\epsilon,t)\to 0 \tag{A4}$$

as $\epsilon_0\to 0$, if we chose $\epsilon=\epsilon(\epsilon_0,t)=\sup_i\delta_i$ (the diameters δ_i are functions of ϵ_0 and t), and therefore $L(\epsilon_0,t)$ must also remain finite at vanishing ϵ_0. Hence, from (41), $D=1$. We have therefore shown that, provided no finite time singularities exist over vanishingly small scales, $D>1$ implies $D_H>1$.

[1]K. R. Sreenivasan, R. Ramshankar, and C. Meneveau, "Mixing entrainment and fractal dimensions of surfaces in turbulent flows," Proc. R. Soc. London Ser. A **421**, 79 (1989).

[2]K. R. Sreenivasan, "Fractals and multifractals in fluid turbulence," Annu. Rev. Fluid Mech. **23** 539 (1991).

[3]G. C. North, and D. A. Santavicca, "The fractal nature of premixed turbulent flames," Combust. Sci. Technol. **72**, 215 (1990).

[4]Y. Sakai, I. Nakamura, and S. Liu, "On fractal features of diffusion field in a turbulent jet," Fifth European Turbulence Conference, Siena, Italy, 5–8 July 1994.

[5]E. Villermeaux, "Fast bimolecular reactions in high Reynolds number turbulence: structure of the reactive interface and surface of reaction," Fifth European Turbulence Conference, Siena, Italy, 5–8 July 1994.

[6]J. C. Vassilicos and J. C. R. Hunt, "Fractal dimensions and spectra of interfaces with application to turbulence," Proc. R. Soc. London Ser. A **435**, 505 (1991).

[7]A. A. Wray and J. C. R. Hunt, "Algorithms for classification of turbulent structures," in *Proceedings of IUTAM Symposium on Topological Fluid Mechanics,"* edited by H. K. Moffatt and A. Tsinober (Cambridge University Press, Cambridge, 1990).

[8]M. V. Berry, N. C. Balazs, M. Tabor, and A. Voros, "Quantum maps," Ann. Phys. **122**, 26 (1979).

[9]J. M. Ottino, *Kinematics of Mixing: Stretching, Chaos and Transport* (Cambridge University Press, Cambridge, 1989).

[10]J. C. H. Fung and J. C. Vassilicos, "Fractal dimensions of lines in chaotic advection," Phys. Fluids **11**, 2725 (1991).

[11]R. H. Kraichnan, "Diffusion by a random velocity field," Phys. Fluids **13**, 22 (1970).

[12]I. T. Drummond, S. Duane, and S. R. Horgan, "Scalar diffusion in simulated helical turbulence with molecular diffusivity," J. Fluid Mech. **138**, 75 (1984).

[13]C. Turfus, "Stochastic modelling of turbulent dispersion near surfaces," Ph.D. dissertation, University of Cambridge, United Kingdom, 1985.

[14]M. R. Maxey and S. Corrsin, "Gravitation settling of aerosol particles in randomly oriented cellular flow fields," J. Atmos. Sci. **43**, 1112 (1986).

[15]M. R. Maxey, "The motion of small spherical particles in a cellular flow field," Phys. Fluids **30**, 1915 (1987).

[16]J. C. H. Fung, J. C. R. Hunt, N. A. Malik, and R. J. Perkins, "Kinematic simulation of homogeneous turbulent flows generated by unsteady random fourier modes," J. Fluid Mech. **236**, 281 (1992).

[17]K. J. Falconer, *The Geometry of Fractal Sets* (Cambridge University Press, Cambridge, 1985).

[18]N. Peters, *Twenty-Frst International Symposium on Combustion* (The Combustion Institute, Pittsburgh, 1986), pp. 1231–1250.

[19]J. C. H. Fung, J. C. R. Hunt, R. J. Perkins, A. A. Wray, and D. D. Stretch, "Defining the zonal structure of turbulence using pressure and invariants of the deformation tenor," *Proceedings of the Third European Turbulence Conference,"* Stockholm, 1990, edited by A. V. Johansson and P. H. Alfredsson (Springer-Verlag, Berlin, 1991).

[20]J. C. Vassilicos, "On the geometry of lines in two-dimensional turbulence," in *Advances in Turbulence 2*, edited by H.-H. Fernholz and H. E. Fiedler (Springer-Verlag, Berlin, 1989).

[21]J. C. Vassilicos, "Fractal and moving interfaces in turbulent flows," Ph.D. dissertation, University of Cambridge, United Kingdom, 1990.

[22]R. H. Kraichnan, "Inertial range in two-dimensional turbulence," Phys. Fluids **10**, 1417 (1967).

[23]G. K. Batchelor, "Computation of the energy spectrum in homogeneous two-dimensional turbulence," Phys. Fluids **12**, 233 (1969).

[24]P. G. Saffman, "On the spectrum and decay of random two-dimensional vorticity distributions at large Reynolds number," Stud. Appl. Math. **50**, 377 (1971).

[25]K. J. Falconer, *Fractal Geometry: Mathematical Foundations and Applications* (Wiley, New York, 1990).

[26]G. H. Hardy, "Weierstrass's non-differentiable function," Trans. Am. Math. Soc. **17** 301 (1916).

[27]M. Holschneider and P. Tchamitchian, *Les Ondelettes en 1989*, edited by P. G. Lemarié (Springer-Verlag, Berlin, 1990).

[28]H. Stommel, "Trajectories of small bodies sinking slowly through convection cells," J. Mar. Res. **8**, 24 (1949).

[29]H. Aref, "Stirring by chaotic advection." J. Fluid Mech. **143**, 1 (1984).

[30]G. K. Batchelor, *The Theory of Homogeneous Turbulence* (Cambridge University Press, Cambridge, 1953).

[31]R. W. Hamming, "Stable predictor–corrector methods for ordinary differential equations," J. Assoc. Comput. Mach. **6**, 37 (1959).

[32]W. H. Press, B. P. Flannery, S. A. Teukolsky, and W. T. Vetterling, *Numerical Recipes: The Art of Scientific Computing* (Cambridge University Press, Cambridge, 1986).

[33]B. B. Mandelbrot, *The Fractal Geometry of Nature* (Freeman, New York, 1982).

[34]G. K. Batchelor, "Small-scale variation of convected quantities like temperature in turbulent fluid. Part 1. General discussion and the case of small conductivity," J. Fluid Mech. **5**, 113 (1954).

[35]A. Giorgilli, D. Casati, L. Sironi, and L. Galgani, "An efficient procedure to compute fractal dimensions by box counting," Phys. Lett. A **115**, 5, 202 (1986).

[36]A. N. Kolmogorov, "The local structure of turbulence in incompressible viscous fluid for very large Reynolds numbers," Acad. Sci. USSR **30**, 301 (1986).

[37]G. K. Batchelor, "The effect of homogeneous turbulence on material lines and surfaces," Proc. R. S. London Ser. A **213**, 349 (1952b).

[38]J. C. R. Hunt, S. K. Lele, P. Moin, and A. A. Wray, "Eddies, streams and convergence zones," in *Proceedings of NASA Ames 1988 Summer Program,* 1988.

[39]P. E. Dimotakis and G. L. Brown, "The mixing layer at high Reynolds number: Large-structure dynamics and entrainment," J. Fluid Mech. **78**, 535 (1976).

[40]J. E. Broadwell and R. E. Breidenthal, "A simple model of mixing and chemical reaction in a turbulent shear layer," J. Fluid Mech. **125** (1982).

[41]M. M. Koochesfahani and P. E. Dimotakis, "Mixing and chemical reaction in a turbulent liquid mixing layer," J. Fluid Mech. **170**, 83 (1986).

[42]J. M. Redondo, "The structure of turbulent density interface," Ph.D. dissertation, University of Cambridge, United Kingdom, 1990.

[43]D. J. Carruthers and J. C. R. Hunt, "Velocity fluctuations near an interface between turbulent region and a stably stratified layer," J. Fluid Mech. **165**, 475 (1986).

[44]H. G. E. Hentschel and I. Procaccia, I. "Relative diffusion in turbulent media: The fractal dimension of clouds," Phys. Rev. A **29**, 1461 (1984).

[45]J. C. Vassilicos and J. C. R. Hunt, "Turbulent flamelet propagation," Combust. Sci. Tech. **87**, 291 (1992).

[46]G. K. Batchelor, "Diffusion in a field of homogeneous turbulence: II. The relative motion of particles," Proc. Camb. Philos. Soc. **48**, 345 (1952a).

[47]R. J. Perkins, N. A. Malik, and J. C. H. Fung, "Cloud dispersion models," *Proceedings of the Fourth European Turbulence Conference*, Delft, 1992, edited by F. T. M. Nieuwstadt (Kluwer, New York, 1993).

This article is copyrighted as indicated in the article. Reuse of AIP content is subject to the terms at: http://scitation.aip.org/termsconditions. Downloaded to IP: 155.198.172.98 On: Fri, 12 Jun 2015 13:29:57

[48]R. J. Perkins and J. C. H. Fung, "Dispersion in spatially varying mean flows: An application of the cloud dispersion models," Report to S.A.I.C. Bellevue, Washington, 1993.
[49]J. C. R. Hunt, J. C. Vassilicos, and N. K.-R. Kevlahan, "Turbulence: less a statistical state than a collection of characteristic eddies?," *Seventh Beer sheva International Seminar on MHD flows*, AIAA Progress in Astronautics Series, edited by H. Branover and Y. Unger (AIAA, Washington, DC, 1994).

This article is copyrighted as indicated in the article. Reuse of AIP content is subject to the terms at: http://scitation.aip.org/termsconditions. Downloaded to IP: 155.198.172.98 On: Fri, 12 Jun 2015 13:29:57